

# *Night-time oxidation of surfactants at the air–water interface: effects of chain length, head group and saturation*

Article

Accepted Version

Creative Commons: Attribution 4.0 (CC-BY)

Open Access

Sebastiani, F., Campbell, R. A., Rastogi, K. and Pfrang, C. (2018) Night-time oxidation of surfactants at the air–water interface: effects of chain length, head group and saturation. *Atmospheric Chemistry and Physics*, 18 (5). pp. 3249-3268. ISSN 1680-7316 doi: <https://doi.org/10.5194/acp-18-3249-2018> Available at <https://centaur.reading.ac.uk/72068/>

It is advisable to refer to the publisher's version if you intend to cite from the work. See [Guidance on citing](#).

To link to this article DOI: <http://dx.doi.org/10.5194/acp-18-3249-2018>

Publisher: Copernicus Publications

All outputs in CentAUR are protected by Intellectual Property Rights law, including copyright law. Copyright and IPR is retained by the creators or other copyright holders. Terms and conditions for use of this material are defined in the [End User Agreement](#).

[www.reading.ac.uk/centaur](http://www.reading.ac.uk/centaur)

**CentAUR**

Central Archive at the University of Reading

Reading's research outputs online



1

## 2 **Night-time oxidation of surfactants at the air–water interface: effects of chain length,** 3 **head group and saturation.**

4

5 Federica Sebastiani,<sup>a,b</sup> Richard A. Campbell,<sup>b</sup> Kunal Rastogi<sup>a</sup> and Christian Pfrang.<sup>a\*</sup>6 <sup>a</sup> Department of Chemistry, University of Reading, P.O. Box 224, RG6 6AD, Reading, UK7 <sup>b</sup> Institut Laue-Langevin, 71 avenue des Martyrs, CS20156, 38042 Grenoble Cedex 9, France

8 \* corresponding author: c.pfrang@reading.ac.uk

9

### 10 **Abstract**

11 Reactions of the key atmospheric night-time oxidant NO<sub>3</sub> with organic monolayers at the air–water interface are  
12 used as proxies for the ageing of organic-coated aqueous aerosols. The surfactant molecules chosen for this  
13 study are oleic acid (OA), palmitoleic acid (POA), methyl oleate (MO) and stearic acid (SA) to investigate the  
14 effects of chain length, head group and degree of unsaturation on the reaction kinetics and products formed.  
15 Fully and partially deuterated surfactants were studied using neutron reflectometry (NR) to determine the  
16 reaction kinetics of organic monolayers with NO<sub>3</sub> at the air–water interface for the first time. Kinetic modelling  
17 allowed us to determine the rate coefficients for the oxidation of OA, POA and MO monolayers to be  $(2.8 \pm 0.7)$   
18  $\times 10^{-8}$  cm<sup>2</sup> molecule<sup>-1</sup> s<sup>-1</sup>,  $(2.4 \pm 0.5) \times 10^{-8}$  cm<sup>2</sup> molecule<sup>-1</sup> s<sup>-1</sup> and  $(3.3 \pm 0.6) \times 10^{-8}$  cm<sup>2</sup> molecule<sup>-1</sup> s<sup>-1</sup>,  
19 respectively. The corresponding uptake coefficients were found to be  $(2.1 \pm 0.5) \times 10^{-3}$ ,  $(1.7 \pm 0.3) \times 10^{-3}$  and  
20  $(2.1 \pm 0.4) \times 10^{-3}$ . For the much slower NO<sub>3</sub>-initiated oxidation of the saturated surfactant SA we found a loss  
21 rate of  $(5 \pm 1) \times 10^{-12}$  cm<sup>2</sup> molecule<sup>-1</sup> s<sup>-1</sup> which we consider to be an upper limit for the reactive loss, and  
22 estimated an uptake coefficient of  $(5 \pm 1) \times 10^{-7}$ . Our investigations demonstrate that NO<sub>3</sub> will contribute  
23 substantially to the processing of unsaturated surfactants at the air–water interface during night-time given its  
24 reactivity is ca. two orders of magnitude higher than that of O<sub>3</sub>. Furthermore, the relative contributions of NO<sub>3</sub>  
25 and O<sub>3</sub> to the oxidative losses vary massively between species that are closely related in structure: NO<sub>3</sub> reacts ca.  
26 400 times faster than O<sub>3</sub> with the common model surfactant oleic acid, but only ca. 60 times faster with its  
27 methyl ester MO. It is therefore necessary to perform a case-by-case assessment of the relative contributions of  
28 the different degradation routes for any specific surfactant. The overall impact of NO<sub>3</sub> on the fate of saturated  
29 surfactants is slightly less clear given the lack of prior kinetic data for comparison, but NO<sub>3</sub> is likely to  
30 contribute significantly to the loss of saturated species and dominate their loss during night-time. The retention  
31 of the organic character at the air–water interface differs fundamentally between the different surfactant species:  
32 the fatty acids studied (OA and POA) form products with a yield of ~ 20% that are stable at the interface while  
33 NO<sub>3</sub>-initiated oxidation of the methyl ester MO rapidly and effectively removes the organic character ( $\leq 3\%$   
34 surface-active products). The film-forming potential of reaction products in real aerosol is thus likely to depend  
35 on the relative proportions of saturated and unsaturated surfactants as well as the head group properties.  
36 Atmospheric lifetimes of unsaturated species are much longer than those determined with respect to their  
37 reactions at the air–water interface, so that they must be protected from oxidative attack e.g. by incorporation  
38 into a complex aerosol matrix or in mixed surface films with yet unexplored kinetic behaviour.

39

40 **Keywords:** aerosol surface, kinetics, atmospheric reactions, air–water interface, oleic acid, palmitoleic acid,  
41 methyl oleate, stearic acid, nitrate radicals, oxidation, neutron reflectometry.

42

43



## 1 1. Introduction

2 Over the last decades, aerosols have attracted increasing attention from the scientific community because their  
3 impact on the Earth's radiative balance and on cloud formation is still largely unknown (Shindell et al., 2009;  
4 Stevens et al., 2009; Stocker et al., 2013). Atmospheric aerosols derive from natural processes (e.g. volcanoes,  
5 wind-blown dust and sea-spray) and from human activities (e.g. combustion and cooking). A key feature for the  
6 aerosol behaviour is the presence of organic material both in the bulk and at the surface (Fuzzi et al., 2006).  
7 Organic compounds contained in atmospheric aerosols are often surface-active, such as fatty acids. Atmospheric  
8 fatty acids include saturated (such as palmitic acid; Adams & Allen, 2013) as well as unsaturated acids e.g. oleic  
9 acid which is found as component of marine (Tervahattu et al., 2002a; Tervahattu et al., 2002b; Fu et al., 2013)  
10 and cooking (Allan et al., 2010) aerosol. Cooking emissions have been estimated to contribute ca. 10% to the  
11 man-made emission of small particulate matter (PM<sub>2.5</sub>) at 320 mg per person per day based on measurements in  
12 London (Ots et al., 2016). The composition and lifetime of aerosol particles in the atmosphere are largely  
13 determined by the ageing process due to exposure to trace gases, such as NO<sub>3</sub>, OH, O<sub>3</sub> or other oxidants (e.g. Cl  
14 and Br; Estillore et al., 2016). To study the aerosol ageing it is crucial to investigate the heterogeneous reactions  
15 occurring between the particles and gas-phase oxidants. While homogeneous chemistry is well described at the  
16 molecular level, the study of heterogeneous reactions remains a major challenge. Field measurements suggest  
17 that heterogeneous reactions may change the chemical composition of particles and in particular of their surface  
18 films (Robinson et al., 2006). The reactions may alter important properties of the particles like aerosol  
19 hydrophilicity, toxicity and optical properties. Most of the studies to date have investigated the heterogeneous  
20 reaction of organic aerosols by O<sub>3</sub> and OH, which are the main oxidants during daytime. During night-time,  
21 [OH] is very low while the concentration of the photo-labile NO<sub>3</sub> will build up and becomes significant.  
22 Therefore while OH controls the chemistry of the daytime atmosphere, NO<sub>3</sub> radicals have a similar role during  
23 the night (Wayne et al., 1991; Mora-Diez et al., 2002; Ng et al., 2017). In many cases heterogeneous reactions  
24 have been studied using organic droplets or thick films (e.g. King et al., 2004; Gross et al., 2009). However, it  
25 has been shown that experimental studies of organic molecules self-assembled at the surface of water rather than  
26 purely organic aerosols alone are key to understanding atmospheric ageing of aerosols covered in organic  
27 material (Vesna et al., 2008).

28  
29 In the work presented here organic monolayers at the air–water interface are used as proxies for the organic-  
30 coated aqueous atmospheric aerosols, and their reactions with NO<sub>3</sub> are investigated. The molecules chosen for  
31 this study are oleic acid (OA), palmitoleic acid (POA), methyl oleate (MO) and stearic acid (SA). OA (King et  
32 al., 2004; King et al., 2009; King et al., 2010), POA (Huff Hartz et al., 2007; Pfrang et al., 2011), MO (Hearn et  
33 al., 2005; Zahardis & Petrucci, 2007; Xiao & Bertram, 2011; Pfrang et al., 2014, Sebastiani et al., 2015) and SA  
34 (Sobanska et al., 2015) are popular model systems for atmospheric surfactants. MO, the methyl ester of OA, is a  
35 main component of biodiesel (chemical name: fatty acid methyl esters or ‘FAME’; Wang et al., 2009) likely  
36 leading to an increased atmospheric abundance in the future since up to 7% of FAME is added to standard  
37 petroleum diesel in the EU to reduce greenhouse gas emissions; higher proportions of FAME in petroleum diesel  
38 (10% FAME sold as ‘B10’ and 20% FAME sold as ‘B20’) as well as pure FAME (‘B100’) become increasingly  
39 common fuel alternatives across a number of European countries including Germany, France and Finland.

40



1 This selection of molecules allows the investigation of the effects of chain length, head group and degree of  
2 unsaturation on the reaction kinetics and products formed. The surface excess of the organic molecule during the  
3 oxidation reaction is monitored using neutron reflectometry (NR). NR is a powerful technique that can be used  
4 to determine the surface excess of a deuterated monolayers at the air–ACMW (air contrast matched water)  
5 interface (Lu et al., 2000), and information about reaction mechanisms can even be accessed thanks to partial  
6 deuteration of the surfactant (Thompson et al., 2010; Thompson et al., 2013). Further, the surface composition of  
7 mixed systems can be resolved in situ during dynamic processes by the selective deuteration of different  
8 components (Campbell et al., 2016; Ciumac et al., 2017), and therefore the reaction rates of individual  
9 components in mixtures holds great potential for future studies. In the present work, NR is used effectively to  
10 measure the surface excess of organic material (i.e. the combination of reactants and insoluble, involatile  
11 products) in situ during reactions with gas-phase  $\text{NO}_3$ .

12  
13 The study of heterogeneous reactions of  $\text{NO}_3$  at the air–water interface is made possible thanks to four recent key  
14 advances. First, the high flux and the stability of the neutron reflectometer FIGARO (Campbell et al., 2011) at  
15 the Institut Laue-Langevin (Grenoble, France) is exploited through the acquisition of data at the air–water  
16 interface that is far faster than was previously possible (King et al., 2009; King et al., 2010). Second, surface  
17 excesses down to monolayer coverage on the order of a few percent can now be determined precisely through a  
18 refined method of background treatment (Pfrang et al., 2014). Third, improvements in the sample environment  
19 have been achieved by the design and commissioning of a new reaction chamber that has a gas delivery system  
20 optimised for homogeneous diffusion (Sebastiani et al., 2015). Lastly, rigorous measurements of the oxidant  
21 concentrations and development of a kinetic model (Pöschl et al., 2007; Shiraiwa et al., 2009; Shiraiwa et al.,  
22 2010) to interpret the data have been undertaken. Specifically,  $\text{NO}_3$  is produced in situ by reacting  $\text{O}_3$  with  $\text{NO}_2$ ,  
23 the dependence of  $[\text{NO}_3]$  on the initial  $[\text{NO}_2]$  and  $[\text{O}_3]$  is modelled, and to determine the concentration of  $\text{NO}_3$ ,  
24 the steady state concentrations of  $\text{NO}_2$  and  $\text{N}_2\text{O}_5$  are measured using FTIR spectroscopy as a function of the  
25 initial  $[\text{NO}_2]$ .

26  
27 The analysis of the kinetic experiments required the development of a modelling approach to describe all the  
28 relevant reactions and processes. In order to describe the  $\text{NO}_3$ -initiated oxidation we used a model, which  
29 considers, in addition to reactions, other mechanisms, such as accommodation, desorption, competition for  
30 adsorption sites and transport of the gas-phase species. This model builds on the formalism and terminology of  
31 the PRA framework (Pöschl et al., 2007). It is a combination of K2–SURF (Shiraiwa et al., 2009) and KM–SUB  
32 (Shiraiwa et al., 2010), but has been adapted to a planar geometry. KM–SUB and K2–SURF have been applied  
33 to describe a range of experimental datasets and conditions (e.g. Pfrang et al., 2011). Both models describe the  
34 evolution of the kinetic parameters of an organic droplet exposed to oxidants. We have adapted the model to a  
35 monomolecular organic layer at the air–water interface for analysis and interpretation of the experimental data  
36 presented here. The kinetic analysis of the measured surface excess decays for the four reaction systems provides  
37 information on the rate coefficients of the heterogeneous reaction as well as indirect information on the  
38 formation of surface-active products. The results obtained for the different molecules will be discussed in  
39 relation of their chemical structures. Furthermore, the comparison between  $\text{NO}_3$  and other oxidants species  
40 indicates to what extent night-time oxidation is important to atmospheric aerosol ageing. We also estimated



1 oxidant uptake coefficients and compared those to literature data on similar organic molecules that have been  
2 studied in the condensed phase (i.e. droplets or thick films; King et al., 2004 and Gross et al., 2009).

3

## 4 2. Methods

### 5 2.1. Experimental

#### 6 2.1.1 Materials

7 The organic monolayers comprised either deuterated oleic acid ( $d_{34}$ OA,  $\text{CD}_3(\text{CD}_2)_7\text{CD}=\text{CD}(\text{CD}_2)_7\text{CO}_2\text{D}$ , Sigma-  
8 Aldrich, isotopic purity  $\geq 98\%$ , purity 99%), partially deuterated palmitoleic acid ( $d_{14}$ POA,  
9  $\text{CH}_3(\text{CH}_2)_5\text{CH}=\text{CH}(\text{CD}_2)_7\text{CO}_2\text{H}$ , custom-synthesised by the Oxford Deuteration Facility), deuterated methyl  
10 oleate ( $d_{33}$ MO,  $\text{CD}_3(\text{CD}_2)_7\text{CD}=\text{CD}(\text{CD}_2)_7\text{CO}_2\text{CH}_3$ , custom-synthesised by the Oxford Deuteration Facility, ~  
11 95%) and deuterated stearic acid ( $d_{35}$ SA,  $\text{CD}_3(\text{CD}_2)_{16}\text{CO}_2\text{H}$ , Sigma-Aldrich, isotopic purity 98%, purity 99%);  
12 further details may be found in section 1 of the ESI. The subphase was a mixture of 8.1% by volume  $\text{D}_2\text{O}$   
13 (Sigma Aldrich) in pure  $\text{H}_2\text{O}$  (generated using a Millipore purification unit, 18.2 M $\Omega$  cm), known as air contrast  
14 matched water (ACMW). Chloroform (Sigma-Aldrich, > 99.8%) and  $\text{O}_2$  (Air Liquide, France, > 99.9%) were  
15 used as supplied.  $\text{NO}_2$  was supplied in small gas cylinders (112 dm<sup>3</sup>) by Scientific and Technical Gases Ltd  
16 (Newcastle-under-Lyme, UK) and provided as a mixture with synthetic air at a concentration of 1000 ppm with  
17 an analytical tolerance of  $\pm 2\%$ .

18

#### 19 2.1.2 Gas Delivery

20 Nitrate radicals,  $\text{NO}_3$ , were produced *in situ* from the reaction of  $\text{O}_3$  with  $\text{NO}_2$ .  $\text{O}_3$  was generated by the exposure  
21 of molecular oxygen to UV light (the procedure has been described elsewhere; Pfrang et al., 2014).  $[\text{NO}_3]$  was  
22 regulated by changing the flow rate of  $\text{NO}_2$  in the range 0.06 – 0.36 dm<sup>3</sup> min<sup>-1</sup> while  $[\text{O}_3]$  was kept constant at  
23 3.9 ppm (i.e. using a constant UV exposure of the  $\text{O}_2$  molecules and a fixed  $\text{O}_2$  flow rate of 1.2 dm<sup>3</sup> min<sup>-1</sup>). A  
24 flow of the  $\text{NO}_3$ - $\text{NO}_2$ - $\text{N}_2\text{O}_5$ - $\text{O}_2$  mixture was then admitted to the reaction chamber (Sebastiani et al., 2015) and  
25 the organic monolayer was oxidised at a rate that was determined by  $[\text{NO}_3]$ . Measurements of  $\text{NO}_2$  and  $\text{N}_2\text{O}_5$   
26 were carried out using IR absorption spectroscopy to establish the concentrations,  $[\text{NO}_2]$  and  $[\text{N}_2\text{O}_5]$ , and their  
27 uncertainties. Modelling of the well-known reaction scheme allowed the estimation of  $[\text{NO}_3]$ . At a total flow rate  
28 of 1.2 to 1.5 dm<sup>3</sup> min<sup>-1</sup>,  $[\text{NO}_3]$  ranged from  $(3.5 \pm 1.5) \times 10^8$  (13  $\pm$  5 ppt) to  $(4.4 \pm 0.8) \times 10^9$  molecule cm<sup>-3</sup> (160  
29  $\pm$  30 ppt) in the experiments presented here. Further details on the gas flow system as well as the  $\text{NO}_3$  modelling  
30 may be found in Sections 2 and 3 of the ESI.

31

#### 32 2.1.3 Neutron Reflectometry (NR)

33 Only a brief description of the physical basis of NR with reference to its application is given here and an  
34 example of the raw data and their reduction can be found in Section 4 of the ESI. NR measurements of the  
35 oxidation of deuterated monolayers by  $\text{NO}_3$  in the reaction chamber (Sebastiani et al., 2015) were carried out on  
36 FIGARO at the Institut Laue-Langevin (Campbell et al., 2011). High flux settings were used to maximise the  
37 data acquisition rate involving an incident angle of 0.62°, a wavelength range of 2 – 20 Å, and a constant  
38 resolution in momentum transfer,  $q$ , of 11% over the probed  $q$ -range of 0.007 to 0.07 Å<sup>-1</sup>, where  $q =$   
39  $4\pi \sin \vartheta / \lambda$ .



1

2 The time-of-flight mode allowed us to follow the change in reflectivity of a deuterated monolayer at the air–  
3 water interface simultaneously over the whole  $q$ -range with respect to the time of the oxidation reaction. For a  
4 deuterated surfactant monolayer at the air–ACMW interface the reflectivity,  $R$ , can be expressed by:

$$5 \quad R \cong \frac{16\pi^2}{q^4} 4b^2 n^2 \sin^2 \left( \frac{qd}{2} \right) \quad (1)$$

6 where  $b$  is the scattering length of the surfactant, in fm,  $n$  is the number density, in  $\text{\AA}^{-3}$ ,  $d$  is the thickness of the  
7 layer in  $\text{\AA}$ , and  $bn = \rho$  is the scattering length density. We obtained the values of  $\rho$  by fitting the  $R(q)$  curves for  
8 each acquisition to an air–monolayer–ACMW stratified layer model.  $d$  was kept fixed at the value obtained by  
9 fitting a  $R(q)$  curve that we recorded over a wider  $q$ -range (up to  $0.25 \text{\AA}^{-1}$ ). Once  $\rho d$  was determined the surface  
10 excess,  $\Gamma$ , was calculated by:

$$11 \quad \Gamma = \frac{1}{A_{hg}} = \frac{\rho d}{b} \quad (2)$$

12 where  $A_{hg}$  is the area per molecule (or per head group). The value of  $\Gamma$  is very insensitive to specific details of  
13 the approach applied in the  $q$ -range measured, i.e. changing the thickness or density of the film within reasonable  
14 boundaries to account for changes in the surface excess resulted in an uncertainty of  $< 1\%$  monolayer coverage,  
15 because even though  $\rho$  and  $d$  are model dependent they vary inversely when the neutron reflectivity is restricted  
16 to values of  $q < 0.07 \text{\AA}^{-1}$ . Normalisation of the reflectivity data was carried out with respect to the total  
17 reflection of an air–D<sub>2</sub>O measurement. The sample stage was equipped with passive and active anti-vibration  
18 control. The reaction chamber was mounted on the sample stage, it was interfaced with the gas setup, and the  
19 trough was filled with 80 ml of ACMW. A given amount of solution was spread using a microlitre syringe in  
20 order to form the monolayer. The solvent was allowed to evaporate before closing the chamber. Data were  
21 recorded for a few minutes before NO<sub>3</sub> was admitted into the chamber. The time resolution was 2 s. The  
22 alignment of the interface was maintained to a precision of 5  $\mu\text{m}$  using an optical sensor (LKG-152, Keyence,  
23 Japan), which operated through the laser alignment window of the reaction chamber (Sebastiani et al., 2015).

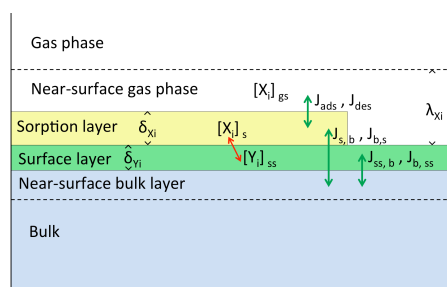
24

## 25 2.2. Kinetic modelling

26 Oxidation of organic compounds by NO<sub>3</sub> may proceed via several reaction channels: rapid addition to the double  
27 bond of unsaturated species as well as slower abstraction of hydrogen atoms particularly relevant for saturated  
28 compounds (Wayne et al., 1991). These mechanisms as well as transport processes need to be considered in  
29 order to fit our experimental data. Based on the PRA-framework (Pöschl et al., 2007; Shiraiwa et al., 2009;  
30 Shiraiwa et al., 2010; Pfrang et al., 2010; Shiraiwa et al., 2012a), a specific model has been developed for the  
31 heterogeneous reaction of a monomolecular organic layer at the air–water interface. The oxidant loss due to the  
32 reaction and transport to the bulk water has been taken into account. The organic reactants used in the  
33 experiments show a very low solubility and slow diffusion in water, hence the loss due to transport to the bulk  
34 could be neglected. The product branching ratios of the heterogeneous reactions are not known, and we were not  
35 able to identify individual product compounds from a monomolecular film at the air–water interface. The  
36 products were thus divided into three categories: volatile, soluble and surface-active species. The distinction  
37 between soluble and volatile species is made on the basis of the product yields reported previously (Hung et al.,  
38 2005; Docherty & Ziemann, 2006) for bulk reaction and considering vapour pressures (Compermolle et al., 2011)  
39 and solubilities (Kuhne et al., 1995) of the products. Because of the method used to produce NO<sub>3</sub> (see ESI



1 Sections 2–3) the ratio  $[\text{NO}_2]/[\text{NO}_3]$  increases from  $10^5$  to  $10^7$  as  $[\text{NO}_3]$  decreases from  $10^9$  to  $10^8$  molecule  
 2  $\text{cm}^{-3}$ . Since  $\text{NO}_2$  can adsorb and desorb from the organic layer (compare King et al., 2010), occupying reactive  
 3 sites, the loss of organic material due to reaction with  $\text{NO}_3$  may also be affected. In particular, for high ratios the  
 4 reactant loss rate will be lower than the loss rate recorded for the lower  $[\text{NO}_2]/[\text{NO}_3]$  ratios. To take this effect  
 5 into account we included the adsorption and desorption of  $\text{NO}_2$  in the model, following the approach used by  
 6 Shiraiwa et al. (2009) The system has been modelled as a gas phase (g) and a near-surface gas phase (gs), above  
 7 a sorption layer (s), a surface layer (ss), a near-surface bulk (nb) and the bulk (b), following the formalism of  
 8 Shiraiwa et al. (2010) (as illustrated in Figure 1).



9  
 10 **Figure 1.** Kinetic model for an organic layer at the air–water interface,  $\delta_{X_i}$  and  $\delta_{Y_i}$  are the thicknesses of  
 11 sorption and surface layer.  $\lambda_{X_i}$  is the mean free path of  $X_i$  in the gas phase. The red arrow shows chemical  
 12 reactions. The green arrows show the transport fluxes.

13 The gas-phase species can adsorb to the sorption layer and interact with the organic molecules in the surface  
 14 layer. The products can stay at the surface layer, or they can be lost through solubilisation into the bulk or by  
 15 evaporation into the gas phase.

16 The evolution of the gas species surface concentration,  $[X_i]_s$ , can be described by taking into account the  
 17 following processes: adsorption, desorption, transport and reaction. Full details are given in the ESI. In the  
 18 following section, only the key equations that describe the reactions are discussed (the nomenclature used is  
 19 based on the PRA framework; Pöschl et al., 2007; Shiraiwa et al., 2009; Shiraiwa et al., 2010; Pfrang et al.,  
 20 2010; Shiraiwa et al., 2012a).

21 Our gas-phase species  $\text{NO}_3$  reacts with the organic layer and the loss,  $L_{\text{surf},Y,\text{NO}_3}$ , can be described with the  
 22 second-order rate coefficient  $k_{\text{surf},Y,\text{NO}_3}$ :

$$23 \quad L_{\text{surf},Y,\text{NO}_3} = k_{\text{surf},Y,\text{NO}_3} [Y]_{\text{ss}} [\text{NO}_3]_s \quad (3)$$

24 The evolution of the  $\text{NO}_3$  and  $\text{NO}_2$  surface and bulk concentrations can be described as follows:

$$25 \quad \frac{d[\text{NO}_3]_s}{dt} = J_{\text{ads},\text{NO}_3} - J_{\text{des},\text{NO}_3} - L_{\text{surf},Y,\text{NO}_3} + J_{\text{bs},\text{NO}_3} - J_{\text{sb},\text{NO}_3} \quad (4)$$

$$26 \quad \frac{d[\text{NO}_3]_b}{dt} = (J_{\text{sb},\text{NO}_3} - J_{\text{bs},\text{NO}_3}) \frac{A}{V} \quad (5)$$

27 where  $A$  is the water surface area and  $V$  is the total water volume. The flux of desorption,  $J_{\text{des},\text{NO}_3}$ , is  
 28 proportional to the inverse of the desorption lifetime,  $\tau_{\text{d},\text{NO}_3,\text{eff}}^{-1}$ , which it is a combination of two desorption





1 lifetimes, depending on the organic molecule packing at the interface,  $\theta_{ss} = [\text{NO}_3]_s(t)/[\text{NO}_3]_s(0)$ ; either  
 2 closely packed ( $\tau_{d,\text{NO}_3,1}^{-1}$ ), or in the gas-like state ( $\tau_{d,\text{NO}_3,2}^{-1}$ ):

$$3 \quad J_{\text{des},\text{NO}_3} = k_{d,\text{NO}_3}[\text{NO}_3]_s = \tau_{d,\text{NO}_3,\text{eff}}^{-1}[\text{NO}_3]_s \quad (6)$$

$$4 \quad \tau_{d,\text{NO}_3,\text{eff}}^{-1} = \theta_{ss}\tau_{d,\text{NO}_3,1}^{-1} + (1 - \theta_{ss})\tau_{d,\text{NO}_3,2}^{-1} \quad (7)$$

5 The organic reactant, Y, (e.g. oleic acid) can be lost just through reaction with  $\text{NO}_3$  at the surface, hence it is  
 6 described as:

$$7 \quad \frac{d[Y]_{ss}}{dt} = -k_{\text{surf},Y,\text{NO}_3} [Y]_{ss} [\text{NO}_3]_s \quad (8)$$

8 The products (Z) of the heterogeneous reaction cannot be identified individually at the air–water interface by the  
 9 experimental techniques used, hence we divided them in three main categories: surface-active (i.e. remaining at  
 10 the surface,  $Z_S$ ), volatile (i.e. escaping into the gas-phase,  $Z_G$ ) and soluble (i.e. accumulating the droplet bulk,  
 11  $Z_B$ ) species. Since the surface-active products ( $Z_S$ ) will remain at the air–water interface, the surface–bulk  
 12 transport is neglected:

$$13 \quad \frac{d[Z_S]_{ss}}{dt} = c_S k_{\text{surf},Y,\text{NO}_3} [Y]_{ss} [\text{NO}_3]_s \quad (9)$$

14 where  $c_S$  is the branching ratio for the surface-active products. The volatile products ( $Z_G$ ) will leave the surface  
 15 depending on their vapour pressures, but with a lack of information on the chemical composition, we decided to  
 16 use a first-order loss rate coefficient,  $k_{\text{loss},G}$ , to describe the overall effect, hence the differential equation for  $Z_G$   
 17 is:

$$18 \quad \frac{d[Z_G]_{ss}}{dt} = c_G k_{\text{surf},Y,\text{NO}_3} [Y]_{ss} [\text{NO}_3]_s - k_{\text{loss},G} [Z_G]_{ss} \quad (10)$$

19 where  $c_G$  is the branching ratio relative to the volatile products. The bulk–surface transport is not considered for  
 20 the volatile products because it is assumed to be negligible compared to the volatilisation process. The soluble  
 21 products ( $Z_B$ ), once formed, will diffuse into the water bulk depending on the diffusion coefficient,  $D_{b,B}$ , and the  
 22 transport velocity can be estimated as  $k_{bss,B} \approx 4 D_{b,B} / \pi \delta_B$ , where  $\delta_B$  is the effective molecular diameter of the  
 23 soluble species. The inverse process is described by a surface–bulk transport velocity  $k_{ssb,B} \approx k_{bss,B} / \delta_B$ , hence  
 24 the evolution of the soluble product concentration in surface layer (ss) and bulk (b) is expressed as:

$$25 \quad \frac{d[Z_B]_{ss}}{dt} = c_B k_{\text{surf},Y,\text{NO}_3} [Y]_{ss} [\text{NO}_3]_s + k_{bss,B} [Z_B]_b - k_{ssb,B} [Z_B]_{ss} \quad (11)$$

$$26 \quad \frac{d[Z_B]_b}{dt} = (k_{ssb,B} [Z_B]_{ss} - k_{bss,B} [Z_B]_b) \frac{A}{V} \quad (12)$$

27 where  $c_B$  is the branching ratio for the soluble products. The equations (4)–(12) describe the evolution of the  
 28 various species. This system of equations cannot be solved analytically, hence the ODE solver of MATLAB  
 29 (2011) has been used for numeric solving. In order to fit  $\Gamma(t)$ , provided by NR, a minimisation of the value of  $\chi^2$   
 30 has been performed using the FMINUIT package (Allodi).

31

### 32 3. Results

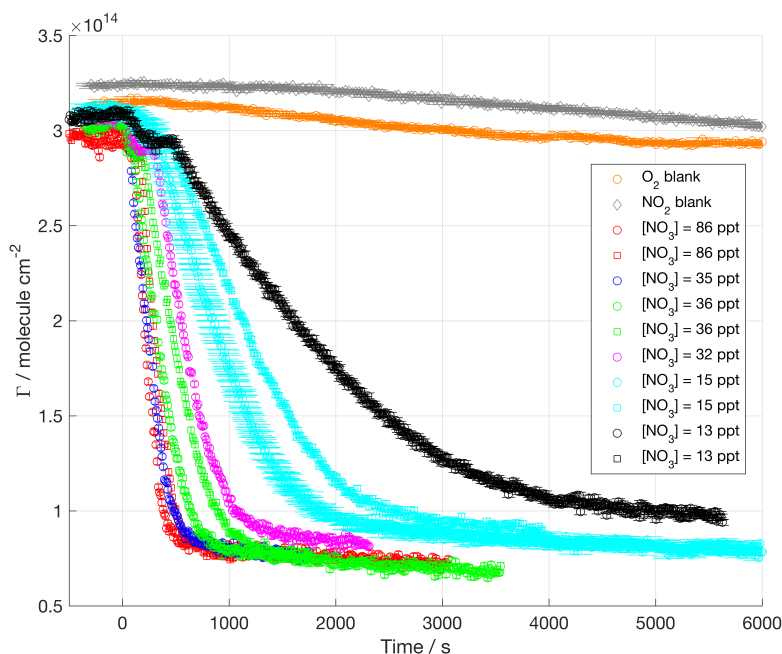
33 Three of the organic molecules considered in this work (OA, POA and MO) contain one unsaturated C=C bond  
 34 in the aliphatic tail while one molecule (SA) is fully saturated. Among the unsaturated surfactants, POA has a



1 shorter tail than OA and MO, whereas MO is a methyl ester in comparison with the fatty acids OA and POA.  
2 The double bond is expected to be the key reactive site for  $\text{NO}_3$ . Kinetic data on the three reactive unsaturated  
3 surfactants are presented first in Sections 3.1 to 3.3, respectively. Furthermore, in a separate process  $\text{NO}_3$  is  
4 known to abstract hydrogen atoms from the aliphatic tail of organic molecules (Shastri & Huie, 1990; Wayne et  
5 al., 1991; Mora-Diez et al., 2002). In order to investigate this effect as well, kinetic data on the saturated  
6 surfactant is then presented in Section 3.4.

### 7 8 **3.1. Oleic acid ( $d_{34}\text{OA}$ ) exposed to nitrate radicals ( $\text{NO}_3$ )**

9 Figure 2 shows the surface excess decays of  $d_{34}\text{OA}$  monolayers at the air-ACMW interface as a function of time  
10 with respect to  $[\text{NO}_3]$ . The  $\text{NO}_3$ -initiated oxidation leads to a non-zero surface excess value ( $7\text{--}10 \times 10^{17}$   
11 molecule  $\text{m}^{-2}$ ) at the end of the reaction. This plateau value is reached after an initial decay, which lasts between  
12 5 min and over 1 h depending on  $[\text{NO}_3]$ .  $[\text{NO}_3]$  ranges from  $(13 \pm 6)$  to  $(86 \pm 45)$  ppt. For several gas conditions,  
13 the oxidation was carried out twice, demonstrating a good reproducibility for high  $[\text{NO}_3]$  ( $> 35$  ppt), and higher  
14 variability for lower concentrations. However, the uncertainty in  $[\text{NO}_3]$ , for  $[\text{NO}_3] < 35$  ppt, is  $\sim 30\%$ , which  
15 means that even a small variation in concentration produces a measurable change in the rate of loss of material.  
16 For example, such an effect can explain the differences of the  $d_{34}\text{OA}$  loss rates recorded for  $[\text{NO}_3] = 15$  ppt. The  
17 oxidant flows in the chamber at  $t = 0$  s, but the decays of the surface excess show a delayed loss most clearly  
18 seen at low  $[\text{NO}_3]$  (black traces with  $[\text{NO}_3] = 13$  ppt). The duration of this initial plateau is longer when the  
19 oxidant concentration is lower. This suggests that some lenses of oleic acid may be floating on top of the  
20 monolayer, and they act as a reservoir for the monolayer until they are totally consumed, then the decay visible  
21 by NR relates only to the monolayer. Brewster angle microscopy (BAM) images, recorded while the OA  
22 monolayer was compressed, show the appearance of lenses, which are not visible in the expanded phase (see  
23 ESI). The surface excess of  $d_{34}\text{OA}$  was monitored as well for exposure to  $\text{O}_2$  and  $\text{NO}_2$  in order to assess a  
24 mechanical loss due to gas flux and isomerisation effects due to the presence of  $\text{NO}_2$  (King et al., 2010).

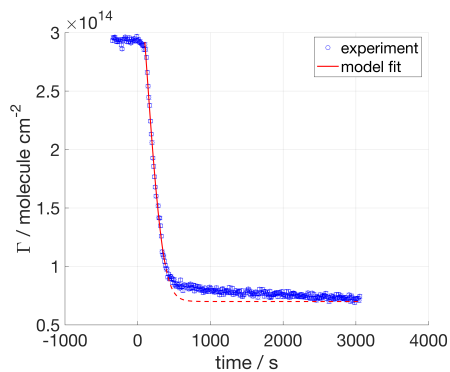


1

2 **Figure 2.** Surface excess decays of oleic acid ( $d_{34}OA$ ) exposed to different  $[NO_3]$ ; mean values of  $NO_3$  mixing  
3 ratios are displayed in the legend (1 ppt =  $2.7 \times 10^7$  molecule  $cm^{-3}$ ).  $NO_3$  is admitted at  $t = 0$  s.

4

5 The kinetic fitting was performed taking into account the variability of the gas concentrations (both for  $NO_3$  and  
6  $NO_2$ ) and the initial surface excess was set to a suitable value to take into account the presence of oleic acid  
7 droplets and their contribution to products. An example of the kinetic fit is displayed in Figure 3 (see ESI for the  
8 complete data set).

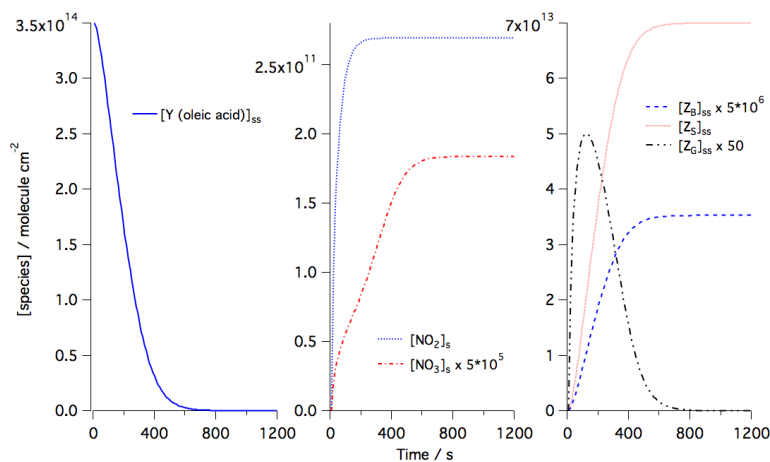


9

10 **Figure 3.** Oleic acid ( $d_{34}OA$ ) exposed to  $[NO_3] = 86$  ppt. The red line illustrates the fit obtained from our kinetic  
11 modelling. The solid section of the red line indicates the data range used for the optimisation of the kinetic  
12 parameters; the dashed section of this line illustrates the modelled final part of the decay, but these data were not  
13 used in the optimisation of the fitting since below a certain surface excess the molecules rearrange with a  
14 different orientation in respect to the interface. The experimental data are displayed with error bars but they are  
15 of the same scale as the marker size and hence not very visible; these experimental uncertainties were used in the  
16 fitting procedure to calculate the value of  $\chi^2$ .



1 The range of data used for the kinetic fitting starts after the initial plateau, and ends at  $1 \times 10^{14}$  molecule  $\text{cm}^{-2}$ ;  
 2 data below this value are excluded from the fitting on the assumption that below a certain surface excess the  
 3 surfactant molecules reorient at the interface and the proportion of surface-active products becomes significant  
 4 (Pfrang et al., 2014) affecting the validity of the fit in this region. The fitted curve, which results from the sum of  
 5 the surface excesses of  $d_{34}\text{OA}$  and the products, is shown as a solid red line in Figure 3. Since NR effectively  
 6 measures the quantity of deuterium atoms at the air–ACMW interface, a distinction between reactant and  
 7 products is not possible; hence the fitting function needs to take into account the contribution to  $\Gamma$  from both  
 8  $d_{34}\text{OA}$  and its reaction products. In order to determine the product yields, it is assumed that at  $t = 0$  s the signal is  
 9 arising solely from  $d_{34}\text{OA}$ , while the signal for long reaction time (e.g.  $t > 1000$  s for  $[\text{NO}_3] = 86$  ppt) is entirely  
 10 due to the surface-active products. Also, the products (Hung et al., 2005; Docherty & Ziemann, 2006) are  
 11 assumed to have a similar scattering length density to  $d_{34}\text{OA}$ , on the basis that upon oxidation the  $d\text{OA}$  molecule  
 12 is expected to break into two parts (Hung et al., 2005; Docherty & Ziemann, 2006), which each maintains almost  
 13 the same ratio between scattering length and molecular volume. In a first approximation, the scattering length of  
 14 the products is likely to be half of the scattering length of  $d_{34}\text{OA}$  and the product film thickness can be thought to  
 15 be ca. half of the  $d_{34}\text{OA}$  film thickness. Given that and considering Eq. 2, the resulting surface excess of the  
 16 products corresponds to the value calculated with  $\rho$ ,  $d$  and  $b$  of  $d_{34}\text{OA}$ . This approximation is not valid in the  
 17 extreme case of the products being only surface-active, since the packing would be two times denser than that  
 18 for oleic acid, and this should be considered in the surface excess calculation and consequent modelling. In our  
 19 study, the surface-active product yield is 20% and it has been taken into account that the total number of product  
 20 molecules (surface-active, volatile and soluble) was twice the number of the reactant molecules; we have also  
 21 estimated the scattering length densities for the likely products.  
 22



23

24 **Figure 4.** The evolution of the surface concentrations obtained from kinetic modelling using the best-fitted  
 25 parameters for the data shown in Fig. 3 for (a) the organic reactant (Y) in this case oleic acid; (b) the gas-phase  
 26 species  $\text{NO}_3$  and  $\text{NO}_2$ ; and (c) the surface-active ( $Z_S$ ), volatile ( $Z_G$ ) and soluble ( $Z_B$ ) products.

27 The accommodation coefficients for the gas-phase species were fixed to one, and the desorption lifetimes were  
 28 left free to vary in the range  $10^{-9}$ – $10^{-7}$  s, which is in agreement with the values suggested by Shiraiwa et al.  
 29 (2012b). For the rate coefficient,  $k_{\text{surf}}$ , the range of variability was optimised through a preliminary sensitivity



1 study performed by changing in the Matlab code the value of  $k_{\text{surf}}$ . The suitable range of values found was (0.7–  
2  $4) \times 10^{-8} \text{ cm}^2 \text{ molecule}^{-1} \text{ s}^{-1}$ , which is significantly higher than the best fit value provided by Shiraiwa et al.  
3 (2012b) for abietic acid exposed to  $\text{NO}_3$  ( $1.5 \times 10^{-9} \text{ cm}^2 \text{ molecule}^{-1} \text{ s}^{-1}$ ). The optimisation of the kinetic  
4 parameters was performed systematically by the  $\chi^2$  minimisation routine FMINUIT (Allodi).

5

6 This fitting approach has been applied to all the molecules studied, while accounting for different product yields  
7 and kinetic parameter ranges (see Table 1). Modelled evolutions of the concentrations of reactants and products  
8 are exemplified in Figure 4.

9

10 A preliminary analysis of the  $\Gamma(t)$  profiles was needed to choose the kinetic parameters related to the products,  
11 which have been used as fixed input parameters. The product yields were optimised to  $c_{\text{S}} = 0.2$  for the surface-  
12 active products,  $c_{\text{G}} = 0.45$  for the volatile products and  $c_{\text{B}} = 0.35$  for the soluble products. The product yields  
13 were derived from Docherty & Ziemann (2006); the products were assumed to be hydroxy nitrates, carbonyl  
14 nitrates, dinitrates and hydroxydinitrates (Docherty & Ziemann, 2006) as well as a dimer and more highly  
15 nitrated compounds from Hung et al. (see products 2a' and 2b' in Hung et al., 2005). A systematic study was  
16 performed to determine the effect of the loss of volatile and soluble products on the resulting surface excess  
17 profiles. For the volatile products, it was found that a first-order loss rate coefficient,  $k_{\text{loss,G}}$ , above  $1 \times 10^{-1} \text{ s}^{-1}$   
18 does not change the  $\Gamma(t)$  profile and a value of  $5 \times 10^{-1} \text{ s}^{-1}$  was chosen. For the soluble products, the loss will  
19 occur upon diffusion in the sub-phase, hence the relevant parameter is the diffusion coefficient into the bulk  
20 water,  $D_{\text{b,ZB}}$ . The calculated  $\Gamma(t)$  was affected by the presence of soluble products only for values of  $D_{\text{b,ZB}}$  below  
21  $10^{-14} \text{ cm}^2 \text{ s}^{-1}$ ; since no evidence of such an effect was found in the experimental data  $D_{\text{b,ZB}}$  was fixed to  $10^{-7}$   
22  $\text{cm}^2 \text{ s}^{-1}$ . The best fit values for the kinetic parameters related to the heterogeneous reaction between  $d_{34}\text{OA}$  and  
23  $\text{NO}_3$  are summarised in Table 1. The rate coefficient for  $d_{34}\text{OA}-\text{NO}_3$  reaction in presence of  $\text{NO}_2$  and  $\text{O}_2$  is  $(2.8$   
24  $\pm 0.7) \times 10^{-8} \text{ cm}^2 \text{ molecule}^{-1} \text{ s}^{-1}$ . The loss due to  $\text{O}_2$  and/or  $\text{NO}_2$  flows leads to an apparent rate coefficient on  
25 the order of  $10^{-11} \text{ cm}^2 \text{ molecule}^{-1} \text{ s}^{-1}$ , which is well within the uncertainty of the reactive rate coefficient. The  
26 short desorption time for  $\text{NO}_3$  is  $(8.1 \pm 4.0) \times 10^{-9} \text{ s}$  and the slow desorption is about three times longer, similar  
27 to the  $\text{NO}_2$  desorption time. The introduction of two desorption times reflects the change of orientation of the  
28 organic molecules at the interface, i.e. for a highly packed monolayer the reactive site is assumed to be less  
29 accessible, and the oxidant has less affinity for other parts of the molecules hence the desorption is faster. When  
30 the organic surface coverage decreases the reactive sites become more accessible and the desorption is slowed  
31 down. The effect of the two desorption time on the  $[\text{NO}_3]_{\text{s}}$  evolution is visible in Figure 4, where the increase of  
32  $[\text{NO}_3]_{\text{s}}$  shows a different slope from 200 s once the oleic acid surface excess halved (compare to Eq. 7). Figure 4  
33 shows the time evolution of the surface concentrations of reactants, products and gas-phase species; once the  
34 reactant,  $d_{34}\text{OA}$ , is completely consumed all the other species reach a steady state.

35

36

37

38

39



1 **Table 1.** Results of the kinetic modelling of the experimental data for the  $d_{34}\text{OA}-\text{NO}_3$ ,  $d_{14}\text{POA}-\text{NO}_3$ ,  $d_{33}\text{MO}-$   
 2  $\text{NO}_3$  and  $d_{35}\text{SA}-\text{NO}_3$  systems. The uncertainties correspond to one standard deviation.

	Best fit values			
Modelled parameter	$d_{34}\text{OA}$	$d_{14}\text{POA}$	$d_{33}\text{MO}$	$d_{35}\text{SA}$
$k_{\text{surf}} / 10^8 \text{ cm}^2 \text{ molecule}^{-1} \text{ s}^{-1}$	$2.8 \pm 0.7$	$2.4 \pm 0.5$	$3.3 \pm 0.6$	$(5 \pm 1) \times 10^{-4}$
(constraints)	(0.7 – 4)	(1 – 3)	(0.7 – 4)	$(10^{-4} - 4)$
$\tau_{d,\text{NO}_3,1} / 10^9 \text{ s}$	$8.1 \pm 4.0$	$16 \pm 4.0$	$8.1 \pm 3.0$	$18.2 \pm 0.4$
(constraints)	(5 – 20)	(5 – 20)	(5 – 20)	(5 – 20)
$\tau_{d,\text{NO}_3,2} / 10^8 \text{ s}$	$2.3 \pm 0.8$	$3.1 \pm 1.3$	$3.7 \pm 1.3$	$[0.70 \pm 0.01]^a$
(constraints)	(0.7 – 4)	(1 – 6)	(1 – 5)	(0.7 – 4)
$\tau_{d,\text{NO}_2} / 10^8 \text{ s}$	$2.8 \pm 1.6$	$4.7 \pm 2.0$	$2.9 \pm 2.0$	$4.7 \pm 0.4$
(constraints)	(0.1 – 6)	(0.1 – 6)	(0.1 – 6)	(0.1 – 6)

3 <sup>a</sup>  $\tau_{d,\text{NO}_3,2}$  corresponds to the lower limit of the constrained range; in this system the surface excess does  
 4 not halve in the experimentally accessible timeframe and hence  $\tau_{d,\text{NO}_3,2}$  is not accurately determined.  
 5

### 6 3.2. Palmitoleic acid ( $d_{14}\text{POA}$ ) exposed to nitrate radicals ( $\text{NO}_3$ )

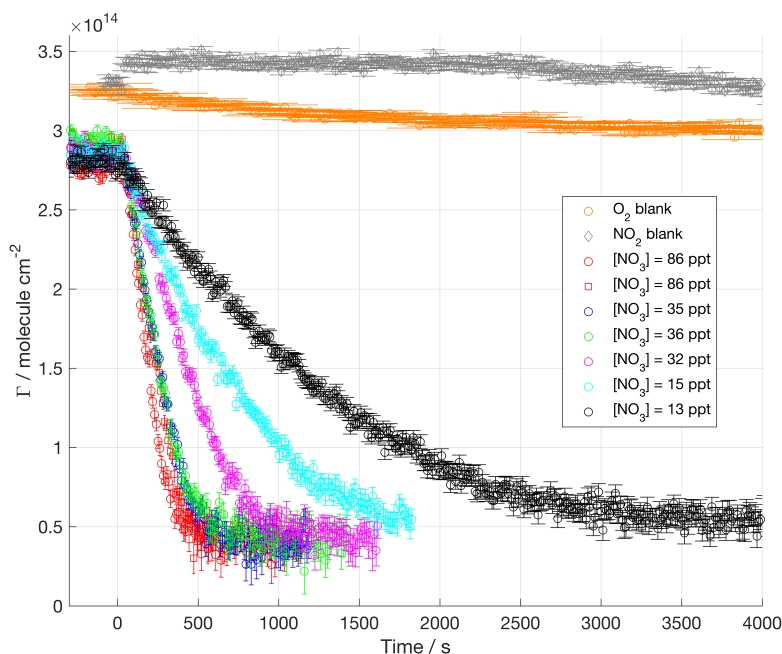
7  $\text{NO}_3$ -initiated oxidation of POA monolayers at the air–water interface was studied as described above for OA.  
 8 14 deuterium atoms were present between the carbon double bond and the carboxylic group in the partially-  
 9 deuterated  $d_{14}\text{POA}$  sample used. POA has a chemical structure that is similar to OA. In fact the portion from the  
 10 carboxylic acid to the C=C bond is exactly the same, while the remaining part of POA chain has just five  $\text{CH}_2$   
 11 units compared to the seven  $\text{CH}_2$  units present in the corresponding part of the OA chain. The key reactive site  
 12 (C=C) for  $\text{NO}_3$ -initiated oxidation is in a similar chemical environment, but the products formed and their fates  
 13 may be different. Products are expected to be analogous to those formed by oleic acid, except that they should be  
 14 slightly more volatile since the alkyl chain is shorter.

15  
 16 Figure 5 shows the surface excess decays of  $d_{14}\text{POA}$  monolayers at the air–ACMW interface as a function of  
 17 time with respect to  $[\text{NO}_3]$ . The reaction leads to a non-zero surface excess in the range  $3 - 7 \times 10^{17}$  molecule  
 18  $\text{m}^{-2}$ , which is slightly lower than the value found for  $d_{34}\text{OA}$ ; this suggests that a proportion of the surface-active  
 19 products is formed of hydrogenous material and hence has a low scattering contrast to the neutron probe. The  
 20 proportion of molecules remaining stably at the interface in relation to the number of initial reactant molecules is  
 21 15% for  $d_{14}\text{POA}$  while it is 20 to 25% for  $d_{34}\text{OA}$  (depending on which initial surface excess value is used, fitted  
 22 or measured). On the assumption that the double bond is the reactive site and breaks during the oxidation  
 23 process, the partial deuteration of the  $d_{14}\text{POA}$  (as opposed to the full deuteration of  $d_{34}\text{OA}$ ) may in fact help in  
 24 determining which part of the molecule remains at the interface: 5–10% of the surface-active products appear to  
 25 originate from the alkyl chain not connected to the acidic head group in the  $d_{34}\text{OA}$  system (however, a direct  
 26 proof would require for half-deuterated  $d_{34}\text{OA}$  and/or fully deuterated  $d_{14}\text{POA}$  to become available for additional  
 27 oxidation experiments).

28  
 29 For low oxidant concentrations ( $[\text{NO}_3] < 32$  ppt), the final plateau value was not always reached (although it was  
 30 reached for the slowest reaction) because the reaction had to be stopped prematurely due to time constraints of  
 31 beam time experiments. Compared to  $d_{34}\text{OA}$ , the decay signals are more noisy, which is due to the half  
 32 deuteration leading to a weaker contrast and hence lower signal to noise ratios. The decays of surface excess  
 33 start as soon as  $\text{NO}_3$  is admitted to the chamber and no initial plateau is visible (as was the case for some of the

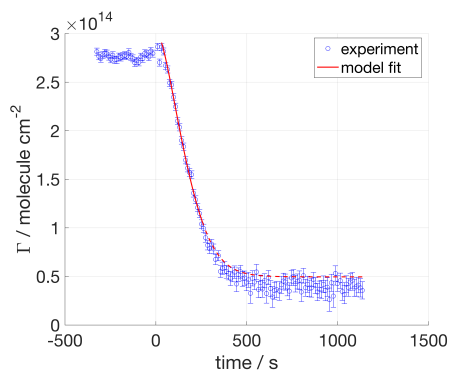


- 1  $d_{34}\text{OA}$  decays displayed in Figure 2). No lenses were formed in this system, as was confirmed by recording
- 2 BAM images while the POA monolayer was compressed (see ESI).



- 3
- 4 **Figure 5.** Surface excess decays of palmitoleic acid ( $d_{14}\text{POA}$ ) exposed to different  $[\text{NO}_3]$ ; mean values are
- 5 displayed in the legend.  $\text{NO}_3$  exposure is started at  $t = 0$  s. The experimental data are more scattered than those
- 6 for  $d_{34}\text{OA}$ , because the  $d_{14}\text{POA}$  was half-deuterated (*i.e.* 14 D atoms, see Table 1 in ESI) leading to a weaker
- 7 contrast (*i.e.* lower signal-to-noise ratio) compared to the fully deuterated molecules studied.

- 8 The kinetic analysis was performed as described for  $d_{34}\text{OA}$ . The input parameters for description of the products
- 9 were  $c_S = 0.17$ ,  $c_G = 0.48$  and  $c_B = 0.35$ , the surface-active and volatile product yields were adjusted to match the
- 10 residual surface excess; please note that hydrogenous surface-active products are not taken into account in this
- 11 context since the experimentally observed signal originates exclusively from the deuterated part of the POA
- 12 molecules. The variable parameters were constrained to the following value ranges:  $k_{\text{surf}}$  was allowed to vary  $(1 -$
- 13  $3) \times 10^{-8} \text{ cm}^2 \text{ molecule}^{-1} \text{ s}^{-1}$ ,  $\tau_{d,\text{NO}_3,1}$   $(5 - 20) \times 10^{-9} \text{ s}$ ,  $\tau_{d,\text{NO}_3,2}$   $(10 - 60) \times 10^{-9} \text{ s}$  and  $\tau_{d,\text{NO}_2}$   $(0.1 - 6) \times 10^{-8} \text{ s}$  (see
- 14 Table 1).



1

2 **Figure 6.** Palmitoleic acid ( $d_{14}$ POA) exposed to  $[\text{NO}_3] = 86$  ppt. The red line illustrates the fit obtained from our  
3 kinetic modelling (the solid section of the line indicates the data range used for the kinetic analysis; the dashed  
4 section of the model line illustrates the calculated final part of the decay, but the corresponding experimental  
5 data were not used in the optimisation of the fitting).

6 In Figure 6 an example of the model fitted to  $d_{14}$ POA data is displayed; the decay is very well represented by the  
7 model. The results of the kinetic modelling for  $d_{14}$ POA are presented in Table 1. While the rate coefficient is  
8 similar to the value found for  $d_{34}$ OA (Table 1),  $\tau_{d,\text{NO}_3,1}$  is double of the value found for oleic acid, which is  
9 consistent with the hypothesis of an easier access to the double bond due to the shorter alkyl chain of  $d_{14}$ POA.  
10  $d_{14}$ POA surface excess data have larger experimental errors than the fully deuterated molecules.

11

### 12 3.3. Methyl oleate ( $d_{33}$ MO) exposed to nitrate radicals ( $\text{NO}_3$ )

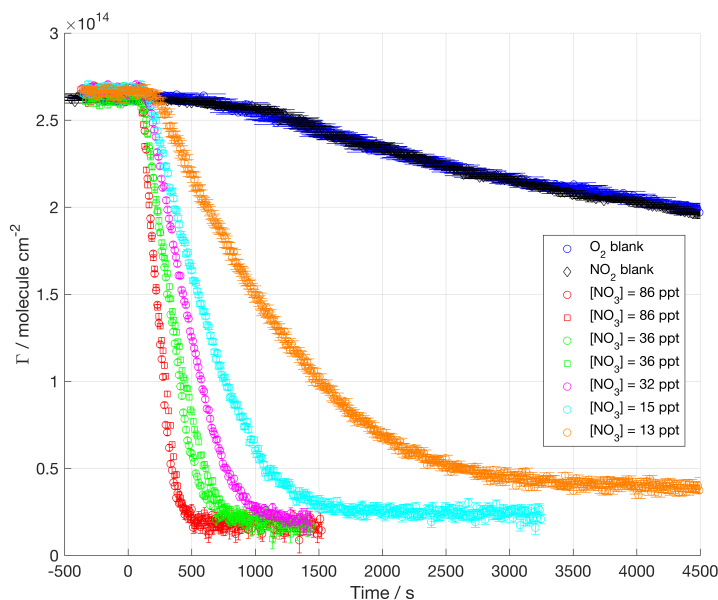
13 Methyl oleate possesses the same aliphatic chain as OA, but it has a different head group: instead of a carboxylic  
14 acid it has a methyl ester ( $\text{COOCH}_3$ ) group. Fully deuterated  $d_{33}$ MO was used (see Table 1 in the ESI). MO  
15 occupies a larger surface area and is less stable at the air–water interface than OA because of its less hydrophilic  
16 head group (see isotherm in Section 1 of the ESI). However, the reactive site is in a similar chemical  
17 environment as for OA, and any difference in reaction kinetics is expected to be related to the chain orientation  
18 and formation of different products.

19

20 Figure 7 displays the surface excess decays of  $d_{33}$ MO monolayers at the air–ACMW interface as a function of  
21 time with respect to  $[\text{NO}_3]$ .  $[\text{NO}_3]$  was varied from  $(13 \pm 6)$  ppt to  $(86 \pm 45)$  ppt.

22

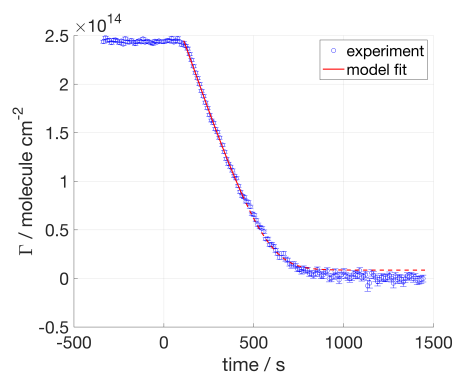




1

2 **Figure 7.** Surface excess of methyl oleate ( $d_{33}\text{MO}$ ) exposed to different  $[\text{NO}_3]$ , mean values are displayed in the  
3 legend.  $\text{NO}_3$  exposure is started at  $t = 0$  s.

4 The kinetic decays presented in Figure 7 show a very clear dependence on  $[\text{NO}_3]$  and very good signal-to-noise  
5 ratios. The decays are generally faster than for both  $d_{34}\text{OA}$  and  $d_{14}\text{POA}$ . The exposure to  $\text{O}_2$  and  $\text{NO}_2$  flow leads  
6 to similar surface excess decays; this non-reactive loss is significantly larger than those recorded for  $d_{34}\text{OA}$  and  
7  $d_{14}\text{POA}$  suggesting that  $d_{33}\text{MO}$  is not as stable at the air–water interface as  $d_{34}\text{OA}$  and  $d_{14}\text{POA}$ . The apparent rate  
8 coefficient obtained for the decays in absence of  $\text{NO}_3$  is about  $2 \times 10^{-10}$  molecule  $\text{cm}^{-2}$   $\text{s}^{-1}$ . As for  $d_{34}\text{OA}$ , the  
9 reaction starts with a slightly increasing delay as the oxidant concentration is lower; the formation of droplets  
10 floating on top of the monolayer after spreading could explain this effect, since the compound is liquid at room  
11 temperature and evidence of lenses was found in BAM images (see Section 1 in the ESI). The minimum value  
12 reached by the surface excess is  $\approx 2 \times 10^{17}$  molecule  $\text{m}^{-2}$ , which is at the detection limit. Therefore, no surface-  
13 active products are expected to remain at the interface as was also found in ozonolysis experiments with  $d_{33}\text{MO}$   
14 in the same chamber (Sebastiani et al., 2015); this was also confirmed by complementary ellipsometry  
15 measurements in the same reaction chamber (data not shown). According to this finding, the product yields were  
16 chosen as follows:  $c_{\text{S}} = 0.03$ ,  $c_{\text{G}} = 0.45$  and  $c_{\text{B}} = 0.52$ . The  $c_{\text{S}}$  value was set to 0.03 in order to account for the  
17 surface excess detection limit considering the experimental background. The kinetic parameters were  
18 constrained to the following value ranges:  $k_{\text{surf}}$  was allowed to vary  $(0.7 - 4) \times 10^{-8}$   $\text{cm}^2$  molecule $^{-1}$   $\text{s}^{-1}$ ,  $\tau_{\text{d,NO}_3,1}$  ( $5$   
19  $- 20$ )  $\times 10^{-9}$  s,  $\tau_{\text{d,NO}_3,2}$  ( $10 - 50$ )  $\times 10^{-9}$  s and  $\tau_{\text{d,NO}_2}$  ( $0.1 - 6$ )  $\times 10^{-8}$  s (see Table 1). An example of the fitting  
20 resulting from the kinetic modelling is displayed in Figure 8. The best-fit values obtained from the kinetic  
21 model are presented in Table 1. The rate coefficient for  $d_{33}\text{MO}$  is slightly larger than those for both  $d_{34}\text{OA}$  and  
22  $d_{14}\text{POA}$ , while the desorption times are similar to those found for  $d_{34}\text{OA}$  and  $d_{14}\text{POA}$  with the exception of the  
23 doubled  $\tau_{\text{d,NO}_3,1}$  for POA further confirming the better accessibility of the double bond for the shorter chained  
24 POA compared to both OA and MO. All fits are presented in the ESI.

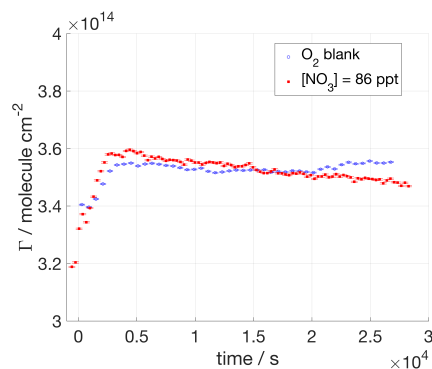


1

2 **Figure 8.** Methyl oleate ( $d_{33}\text{MO}$ ) exposed to  $[\text{NO}_3] = 36$  ppt. The red line illustrates the fit obtained from our  
 3 kinetic modelling (the solid section of the line indicates the data range used for the kinetic analysis; the dashed  
 4 section of the model line illustrates the calculated final part of the decay, but the corresponding experimental  
 5 data were not used in the optimisation of the fitting).

#### 6 3.4 Stearic acid ( $d_{35}\text{SA}$ ) exposed to nitrate radicals ( $\text{NO}_3$ )

7 In addition to adding to the double bond of the unsaturated surfactants discussed in the previous sections,  $\text{NO}_3$   
 8 may abstract hydrogen atoms from the aliphatic tail (Shastri & Huie, 1990; Wayne et al., 1991; Mora-Diez et al.,  
 9 2002). In order to investigate the contribution of this hydrogen abstraction, the saturated surfactant stearic acid  
 10 was exposed to  $\text{NO}_3$ . Figure 9 shows the comparison between the surface excess of a  $d_{35}\text{SA}$  monolayer exposed  
 11 to  $\text{O}_2$  and to  $\text{NO}_3$  at  $(86 \pm 45)$  ppt.



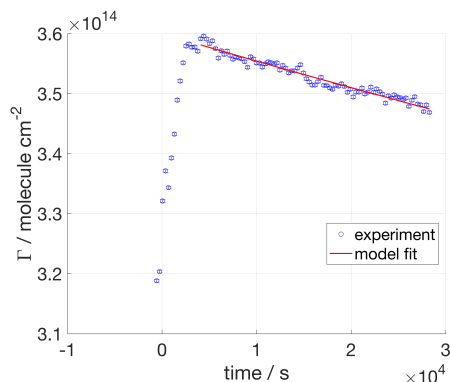
12

13 **Figure 9.** Surface excess of stearic acid ( $d_{35}\text{SA}$ ) exposed to  $\text{O}_2$  (blue circles) and to  $[\text{NO}_3] = 86$  ppt (red filled  
 14 squares). Exposure to  $\text{NO}_3$  starts at  $t = 0$  s. Both surface excess traces show an increase over the first 40 min.  
 15 There is slight subsequent decrease in the surface excess during exposure to  $\text{NO}_3$ .

16 The data were recorded for more than 8 h for both gas-phase environments. The initial surface excess evolution  
 17 of the monolayer exposed to  $\text{NO}_3$  is comparable to that for the  $\text{O}_2$  blank: both profiles show a slow increase in  
 18 surface excess in the first 40 min. Apart from the initial increase in  $\Gamma(t)$  values, no measurable change in the  
 19 surface excess has been recorded when SA is exposed to  $\text{O}_2$ , and the film is shown to be stable on the probed  
 20 time scale; in presence of  $\text{NO}_3$  a slight decrease in surface excess hints at a slow reactive decay. From these data  
 21 we obtained a rate coefficient,  $k_{\text{surf}}$ , of  $(5 \pm 1) \times 10^{-12} \text{ cm}^2 \text{ molecule}^{-1} \text{ s}^{-1}$ ; the parameters ranges and initial values  
 22 in the model were kept as for OA for consistency, because of the lack of any experimental data on products and



1 very limited kinetic data due to the very slow process; the lower limit for the rate coefficient was decreased to  $1$   
2  $\times 10^{-12} \text{ cm}^2 \text{ molecule}^{-1} \text{ s}^{-1}$ ; the model fit to the experimental data is shown in Figure 10. For this system, the  
3 surface coverage never reached below 90% of the initial value and hence the determination of the second  
4 desorption times,  $\tau_{d,\text{NO}_3,2}$ , is not accurate (the value obtained for  $\tau_{d,\text{NO}_3,2}$  actually corresponds to the lower limit of  
5 the constrained range; see value in square brackets in Table 1). It should be noted that in our experimental  
6 approach it is theoretically possible that the chemical composition of the monolayer could change upon reaction  
7 with  $\text{NO}_3$  (e.g. formation of organonitrates; Gross & Bertram, 2009) while the scattering excess (i.e. the product  
8 of  $\rho$  and  $d$  in Eq. (2)) could by coincidence remain unchanged during this process; the resulting  $\Gamma(t)$  plot would  
9 then also remain constant. This is highly unlikely, in particular since our result is in accordance with the findings  
10 of Knopf et al. (2006), where the exposure to  $[\text{NO}_3] = 100 \text{ ppt}$  for one week resulted in a maximum of 10% of  
11 the organic monolayer being volatilised (the monolayer was supported on a solid substrate and the measurement  
12 does not rely on the neutron scattering length density). For practical reasons it is not feasible to carry out NR  
13 experiments on a similar time scale, however our results suggest that the kinetic behaviour may be affected by  
14 the type of substrate given the faster oxidation of  $d_{35}\text{SA}$  observed at the air–water interface during exposure to  
15  $\text{NO}_3$ .



16  
17 **Figure 10.** Stearic acid ( $d_{35}\text{SA}$ ) exposed to  $[\text{NO}_3] = 86 \text{ ppt}$ . The red line illustrates the fit obtained from our  
18 kinetic modelling.

#### 19 4. Discussion

20 The experimental results presented together with the tailored modelling approach for the four structurally  
21 different monolayers has allowed determination of the kinetic parameters of heterogeneous reactions at the air–  
22 water interface with  $\text{NO}_3$  for the first time. The study of heterogeneous reactions of organic monolayers at the  
23 air–water interface exposed to oxidants is crucial to understand the role of such films for the atmospheric fate of  
24 organic-coated aqueous aerosols (Gilman et al., 2004). The studies performed on these type of reactions were  
25 nearly exclusively carried out monitoring the gas-phase species (Wadia et al., 2000; Knopf et al., 2007; Cosman  
26 et al., 2008a; Cosman et al., 2008b). Gross & Bertram (2009) investigated the oxidation of organic monolayers at  
27 an air–solid interface and in addition to monitoring the gas-phase species during the reaction, they analysed the  
28 product film with several surface spectroscopic techniques. The monitoring of the organic monolayer during  
29 oxidation at the air–water interface was introduced by King et al. (2009) for the study of oleic acid exposed to  
30  $\text{O}_3$ . To the best of our knowledge, no-one has investigated the oxidation of organic monolayer at the air–water  
31 interface by  $\text{NO}_3$  by in situ kinetic measurements of the surface excess.



1

2 The kinetic parameters obtained by analysing the NR data allow investigation of the effects of the chemical  
 3 structure, i.e. chain length, degree of unsaturation and head group properties. A summary of the kinetic results  
 4 reported in the present study is given in Table 2. For the unsaturated molecules studied we obtained rate  
 5 coefficients in the order of  $10^{-8} \text{ cm}^2 \text{ molecule}^{-1} \text{ s}^{-1}$ , which leads to uptake coefficients,  $\gamma$ , for  $\text{NO}_3$  on a droplet  
 6 covered in a monolayer of organic compound to be in the order of  $10^{-3}$ . These results broadly agree with the very  
 7 limited number of measurements found in the literature (Moise et al., 2002; Knopf et al., 2006; Gross &  
 8 Bertram, 2009; Xiao & Bertram, 2011; Zhao et al, 2011; Zhang et al., 2014) for unsaturated organics exposed to  
 9  $\text{NO}_3$  in particular when considering that experiments are often carried out in very different conditions (e.g. on a  
 10 gold surface instead of the water surface we used) and employ fundamentally different experimental approaches  
 11 (e.g. flow tubes). Moise et al. (2002) studied the uptake of  $\text{NO}_3$  by a range of liquid or frozen organics in a  
 12 rotating wall flow tube, and they measured uptake between  $1.6 \times 10^{-3}$  and  $1.5 \times 10^{-2}$  depending on the kind of  
 13 liquid organic compounds. Gross & Bertram (2009) determined the uptake of  $\text{NO}_3$  by a self-assembled alkene  
 14 monolayer at the solid substrate obtaining an uptake coefficient of 0.034. They suggested that a possible reason  
 15 for this higher value compared to the results of Moise et al. (2002) is the location of the double bond at the  
 16 interface. Zhang et al. (2014) determined the uptake coefficient of  $\text{NO}_3$  on a model surface of a self-assembled  
 17 monolayer of vinyl-terminated alkanethiols on gold substrate to be  $(2.3 \pm 0.5) \times 10^{-3}$  monitoring the double bond  
 18 rupture. The present results for organic monolayers at the air–water interface are in a better agreement with those  
 19 of Moise et al. (2002) and Zhang et al. (2014). The agreement with Moise et al. (2002) may suggest that the  
 20 accessibility of the reactive site for these monolayers is similar to that of a thick film. However, the work of  
 21 Zhang et al. (2014) was on an organic monolayer at the air–solid interface and the rate of product formation was  
 22 measured instead of the  $\text{NO}_3$  consumption as in Gross & Bertram (2009); in a way our approach is closer to that  
 23 of Zhang et al. (2014), since we followed the organic reactant loss *in situ*. Given the complex chemical  
 24 environments these surfactants will encounter in the atmosphere it would be important to investigate the  
 25 difference in uptake coefficients of  $\text{NO}_3$  by organic monolayers adsorbed to different substrates and compare  
 26 uptake coefficients based on both consumption of  $\text{NO}_3$  and product formation rates.

27

28 **Table 2** Kinetic parameters, uptake coefficients and estimated monolayer lifetimes for the compounds studied.  
 29 Literature values for uptake coefficients on similar compounds are included for comparison.

Surfactant	$k_{\text{surf}} / \text{cm}^2 \text{ molecule}^{-1} \text{ s}^{-1}$	$\gamma / 10^3$	$\gamma_{\text{lit}} / 10^3$	Lifetime <sup>a</sup>
$d_{35}\text{SA}$	$(5 \pm 1) \times 10^{-12}$	$(5 \pm 1) \times 10^{-4}$	$(8.8 \pm 2.5) \times 10^{-1 \text{ b}}$	21 days
$d_{34}\text{OA}$	$(2.8 \pm 0.7) \times 10^{-8}$	$2.1 \pm 0.5$	$(3 \pm 1) \times 10^{2 \text{ c}}$ $[1.6 \pm 0.3] \text{ d}$	6 minutes
$d_{14}\text{POA}$	$(2.4 \pm 0.5) \times 10^{-8}$	$1.7 \pm 0.3$	$[2.3 \pm 0.5] \text{ c}$ $[34^{+44}_{-18}] \text{ f}$	7 minutes
$d_{33}\text{MO}$	$(3.3 \pm 0.6) \times 10^{-8}$	$2.1 \pm 0.4$	$[(1.4^{+8.6}_{-0.5}) \times 10^2] \text{ g}$	5 minutes

30 <sup>a</sup> see Section 4.3 for details on the lifetime calculation;

31 <sup>b</sup> value refers to a self-assembled monolayer on a gold substrate (Knopf et al., 2006);

32 <sup>c</sup> value refers to a study with a flow tube coupled to a chemical ionisation mass spectrometer (Zhao et al., 2011);

33 <sup>d</sup> value refers to 1-octadecene uptake measured in a rotating wall flow tube (Moise et al., 2002);

34 <sup>e</sup> value refers to a vinyl-terminated self-assembled monolayer at a gold surface, which was chosen as a model for  
 35 a double bond positioned at the gas–surface interface by Zhang et al. (2014);

36 <sup>f</sup> value refers to a terminal alkene monolayer at a gold surface (Gross & Bertram, 2009);

37 <sup>g</sup> value refers to binary mixtures of MO and saturated molecules measured in a rotating wall flow tube (Xiao &  
 38 Bertram, 2011).



1

2 The products yields used in our model were based on the findings of Docherty & Ziemann (2006) and Hung et  
3 al. (2005); both papers present possible mechanisms for product formation from the oleic acid droplets reacting  
4 with  $\text{NO}_3$  in presence of  $\text{O}_2$  and  $\text{NO}_2$ .  $\text{NO}_3$  attacks the double bond and the primary reaction is most likely to lead  
5 to the formation of an organonitrate, which would maintain the  $\text{C}_{18}$  chain instead of splitting into  $\text{C}_9$  fragments;  
6 however, subsequent reactions have been found to lead to shorter molecules, such as nonanal and 9-oxononanoic  
7 acid (Docherty & Ziemann, 2006). Organonitrates are reactive species that are likely to undergo further reactions  
8 and produce smaller fragments, which either are lost to the gas- or water-phase or remain at the interface. In  
9 previous work (Hung et al., 2005; Docherty & Ziemann, 2006), the primary organonitrates were found to be  
10 more abundant than shorter fragments, but these studies focused mostly on the first few seconds to minutes of  
11 the reactive degradation, while our work on unsaturated surfactants follows the reaction until the organic film is  
12 fully processed. The surface-active products were found to total 20% and 15% (based on the deuterated  
13 proportion of the molecule only) of the initial amounts of  $d_{34}\text{OA}$  and  $d_{14}\text{POA}$ , while  $d_{33}\text{MO}$  does not lead to any  
14 surface-active products ( $\leq 3\%$ ), probably due to the lower surface activity of the  $\text{COOCH}_3$  head group. The  
15 proportion of volatile and soluble products is mainly based on solubility and volatility estimations (Kuhne et al.,  
16 1995; Compernelle et al., 2011); this distinction was used to predict the time evolution of the concentrations of  
17 these products and their contribution to the surface excess when produced at the interface.  $d_{14}\text{POA}$  is expected to  
18 behave similarly to  $d_{34}\text{OA}$ , except the formation of  $\text{C}_8$  fragments with slightly higher solubility & volatility and  
19 hence a decreased surface-active yield; to our knowledge no studies on  $d_{14}\text{POA}$  exposed to  $\text{NO}_3$  were performed  
20 and no data are available on the products formed.

21

22 The key findings of the present work in relation to surfactant chain length, head group and saturation are  
23 discussed in the following paragraphs.

24

#### 25 4.1. Chain length

26 The slightly lower reactivity towards  $\text{NO}_3$  of  $d_{14}\text{POA}$  compared to  $d_{34}\text{OA}$  is hard to rationalise (the rate  
27 coefficients obtained overlap with the experimental uncertainties), since –if anything– we would have expected  
28  $d_{14}\text{POA}$  to react slightly faster given the fact that the two molecules are identical except a shorter alkyl chain that  
29 could facilitate attack of  $\text{NO}_3$  in the case of  $d_{14}\text{POA}$  (as seems to be the case for  $\text{O}_3$  attack on OA and POA in a  
30 complex 12-component mixture containing these two compounds: Huff Hartz et al. (2007) reported ratios of  
31 effective condensed phase rate constants of  $7 \pm 3$  and  $6 \pm 2$  for POA and OA ozonolysis, respectively; no kinetic  
32 measurements have been reported for the  $d_{14}\text{POA}-\text{O}_3$  system to our knowledge). However, the reactivity  
33 depends on the desorption time as well (Table 1); the longer the lifetime of adsorption, the higher is the  
34 possibility to react;  $\tau_{d,\text{NO}_3,1}$  for  $d_{14}\text{POA}$  is double the value found for  $d_{34}\text{OA}$ , which confirms the hypothesis of an  
35 easier access to the double bond due to the shorter alkyl chain of  $d_{14}\text{POA}$ .

36

37 The uncertainty of the rate coefficient corresponds to the standard deviation of the values found for the rate  
38 coefficients for each oxidant concentration; a lower uncertainty means that the values obtained from the different  
39 oxidant concentrations are closer to each other. Since the rate coefficients obtained for the individual  
40 experiments for  $d_{14}\text{POA}$  agree slightly better than those for the other surfactant reactions, a smaller  $\chi^2$  is obtained



1 despite the clearly visible scatter in the  $d_{14}$ POA surface excess profiles (see Fig. 5) and the larger error bars on  
2 the data.

3

#### 4 **4.2. Head group**

5 The rate coefficients displayed in the second column of Table 2 for the reactions with  $\text{NO}_3$  show a small, but  
6 statistically significant difference between the unsaturated organic compounds investigated:  $d_{33}$ MO reacts  
7 slightly faster than  $d_{34}$ OA with  $d_{14}$ POA reacting the slowest. This order of reactivity is broadly consistent with  
8 that found for the ozonolysis of  $d$ MO (Pfrang et al., 2014; Sebastiani, et al., 2015) and  $d_{34}$ OA (King et al., 2009)  
9 at the air–water interface, but the differences are less pronounced for the more reactive  $\text{NO}_3$ :  $k_{\text{surf},\text{NO}_3} / k_{\text{surf},\text{O}_3}$   
10 ratios are  $\sim 384$  and  $\sim 58$  for  $d_{34}$ OA and  $d_{33}$ MO, respectively.

11

12 A direct comparison between surface excess decays for the three unsaturated surfactants allows us also to  
13 examine if there is a correlation between the type of head group and the presence of products at the air–water  
14 interface. Molecules with a fatty acid (COOH) head group (i.e.  $d_{34}$ OA and  $d_{14}$ POA) left a considerable  
15 proportion of surface-active products at the air–water interface, while  $d_{33}$ MO with its methyl ester (COOCH<sub>3</sub>)  
16 head group did not leave any detectable product ( $\leq 3\%$  surface-active products based on the detection limit for  
17 our experimental set-up). Therefore, the retention of the organic character at the air–water interface differs  
18 fundamentally between the different surfactant species: the fatty acids studied form products with a yield of  $\sim$   
19 20% that are stable at the air–water interface while the  $\text{NO}_3$ -initiated oxidation of the methyl ester rapidly  
20 removes the organic character from the surface of the aqueous droplet. A similar difference (King et al., 2009;  
21 Pfrang et al., 2014; Sebastiani et al., 2015) between methyl ester and parent fatty acid has been found for the  
22 ozonolysis of  $d_{34}$ OA and  $d_{33}$ MO, but the retention of 20% of organic material at the air–water interface is even  
23 more surprising for the more highly reactive nitrate radicals. The film-forming potential of the reaction products  
24 thus strongly depends on the head group properties.

25

#### 26 **4.3. Chain saturation**

27 Unsurprisingly, the fate of the monolayer is altered fundamentally by the absence of unsaturation in the aliphatic  
28 chain. In fact,  $d_{35}$ SA loss from the interface during our 8 h experiments was extremely small, while the initial 40  
29 minutes of reaction lead to an increase of surface excess for both  $\text{NO}_3$  and  $\text{O}_2$ . An increase in surface excess may  
30 depend on a closer packing of the aliphatic chains which is more likely than gas-phase species absorbing to the  
31 interface, since gas absorption was not found for the other molecules studied. Indeed, we have recently reported  
32 an apparent increase in NR signal most likely caused by changes in the structure at the air–water interface for a  
33 two-component mixture of immiscible surfactants (Skoda et al., 2017). Our implementation of NR only at low- $q$   
34 provides a measure of the total neutron scattering excess rather than a direct measure of the surface excess of the  
35 organic material at the interface hence there is a remote possibility that the film composition may be changing  
36 over time due to gas adsorption into the monolayer, e.g. formation of organonitrates by  $\text{NO}_3$  (Gross & Bertram,  
37 2009). Due to limited access to neutron beam time, only one experiment was performed on  $d_{35}$ SA lasting 8 h and  
38 it led to an estimation of the rate coefficient of  $(5 \pm 1) \times 10^{-12} \text{ cm}^2 \text{ molecule}^{-1} \text{ s}^{-1}$ , which is four orders of  
39 magnitude lower than the rate coefficient for the unsaturated molecules. This value has to be considered with  
40 caution, since it relies on the modelling of only one data set, corresponding to the highest  $\text{NO}_3$  concentration,



1 and the parameters in the modelling were the same as for  $d_{34}\text{OA}$  except for the lower limit of the rate coefficient  
2 that has been reduced to  $1 \times 10^{-12} \text{ cm}^2 \text{ molecule}^{-1} \text{ s}^{-1}$ . This was necessary because of the lack of previous  
3 experimental data to constrain the model and the limited reaction extent that could be observed during the  
4 available beam time.

5  
6 The higher stability of SA monolayers upon oxidation compared to the unsaturated molecules suggests that SA  
7 may concentrate at the aerosol surface leading to a stabilisation of the particles. Formation of such a stable film  
8 may protect more reactive species, located within the aerosol bulk (Pfrang et al., 2011), by slowing down the  
9 diffusion of the organic compound from bulk to surface and the diffusion of the oxidant from the gas phase to  
10 the bulk. Accumulation of saturated films in aged organic films has indeed recently been reported (Jones et al.,  
11 2017).

#### 12 13 **4.4. Atmospheric implications**

14 Contrasting the oxidation of  $d_{33}\text{MO}$  upon exposure to  $\text{O}_3$  (Pfrang et al., 2014; Sebastiani, et al., 2015) and  $\text{NO}_3$   
15 shows –as expected– a clearly stronger oxidative power of  $\text{NO}_3$  compared to  $\text{O}_3$ . The oxidative power may be  
16 quantified from the uptake coefficient (Gross & Bertram, 2009) of  $\text{NO}_3$  and  $\text{O}_3$  as the product of uptake  
17 coefficient and gas-phase oxidant concentration.  $\text{O}_3$  is found in the atmosphere at concentration between 10 and  
18 100 ppb. The oxidative power calculated for the lowest concentration would be  $7.5 \times 10^6 \text{ molecule cm}^{-3}$ . For the  
19 calculation of the oxidative power,  $[\text{NO}_3]$  was chosen to be representative of a range of atmospheric mixing  
20 ratios (5–50 ppt, i.e. ca.  $1.4\text{--}13.5 \times 10^8 \text{ molecule cm}^{-3}$ ), which could be encountered in the atmosphere owing to  
21 spatial and seasonal fluctuations (Seinfeld & Pandis, 2006). The resulting oxidative powers are  $1.2 \times 10^6$   
22  $\text{molecule cm}^{-3}$  and  $12 \times 10^6 \text{ molecule cm}^{-3}$  for lowest and highest  $[\text{NO}_3]$ , respectively. Although the  
23 concentration of  $\text{NO}_3$  in the atmosphere is low compared to  $[\text{O}_3]$ , our results suggest that night-time oxidation is  
24 likely to be often dominated by  $\text{NO}_3$ -initiated degradation. This finding suggests that further investigation of the  
25 oxidation driven by  $\text{NO}_3$  is required to understand the fate of aerosol droplets together with studies of the key  
26 daytime oxidant OH. This conclusion is also supported by a very recent study (Jones et al., 2017) suggesting  
27 that atmospheric surfactants are essential inert with respect to ozonolysis making studies of  $\text{NO}_3$  as well as OH-  
28 initiated oxidation even more timely.

29  
30 The lifetime of an organic monolayer is calculated (Moise & Rudich, 2001; Knopf et al., 2011) as the inverse of  
31 the product of  $k_{\text{surf}}$  and  $[\text{NO}_3]_{\text{s}}$ , the  $\text{NO}_3$  surface concentration was calculated as in Smith et al. (2002) using a  
32  $[\text{NO}_3] = 20 \text{ ppt}$  ( $5.4 \times 10^8 \text{ molecule cm}^{-3}$ ). Based on our kinetic experiments, the lifetime with respect to  $\text{NO}_3$ -  
33 initiated oxidation of an organic monolayer of monounsaturated molecules with a surface concentration of  $3 \times$   
34  $10^{14} \text{ molecule cm}^{-2}$  on an aqueous droplet is ca. 5 to 7 minutes, while it becomes about 21 days for saturated  
35 species. Zhao et al. (2011) estimated for a 100 nm droplet of pure oleic acid exposed to 25 ppt  $\text{NO}_3$  a lifetime of  
36 ca. 35 minutes. The direct comparison with our kinetic study on a self-assembled monolayer at the air–water  
37 interface suggests that oleic acid molecules in a pure oleic acid droplet would be degraded ca. 20 times faster  
38 than the same number of oleic acid molecules present in a self-assembled monolayer at the air–water interface of  
39 an aqueous droplet. Self-assembly thus may play a significant role for the kinetic behaviour of surfactant  
40 molecules in the atmosphere. We are currently carrying out experimental studies on oleic-acid based aerosol



1 proxies with complementary techniques (Seddon et al., 2016) to further investigate the importance of complex  
2 self-assembly in atmospheric aerosols.

3

4 The loss of the organic character from the air–water interface will have consequences for the surface tension of  
5 aqueous droplets in the atmosphere: an organic surfactant film substantially reduces the droplet’s surface tension  
6 compared to pure water, so that the film-forming potential of degradation products of these surfactant films is of  
7 key interest. We found that the stability of products formed at the air–water interface differs substantially  
8 between the fatty acids (OA and POA) and the methyl ester (MO) studied. The head group thus seems key to  
9 determine whether the surfactant will be able to reduce the surface tension of water droplets for any considerable  
10 time which could have important consequences for droplet growth and should be considered when developing  
11 emission control strategies.

12

13 The rapid loss of the organic monolayers at the air–water interface demonstrated by our experimental data of the  
14 oxidative decays is surprising given a number of field studies reporting much longer residence times of  
15 unsaturated surfactants in atmospheric aerosols (Morris et al., 2002; Knopf et al., 2005; Ziemann, 2005; Zahardis  
16 & Petrucci, 2007). Such unsaturated organics may have longer lifetimes if protected from oxidative attack by  
17 gas-phase species e.g. inside highly viscous aerosol particles (Virtanen et al., 2010; Pfrang et al., 2011; Shiraiwa  
18 et al., 2011; Shiraiwa et al., 2013) or if mixed with non-reactive species in a complex surface film with yet  
19 unexplored kinetic behaviour. This provides a key motivation to investigate the oxidation of mixed surfactant  
20 films, which represent closer proxies for real atmospheric aerosol droplets in the future. These measurements  
21 have commenced already in our group, and as such the findings presented here provide an essential experimental  
22 basis for an extension of the work and methodology towards an improved understanding of the complex  
23 behaviour of atmospheric aerosols.

24

## 25 **5. Conclusions**

26 We have investigated the reactions of the key atmospheric oxidant  $\text{NO}_3$  with organic monolayers at the air–water  
27 interface as proxies for the night-time ageing of organic-coated aqueous aerosols. The surfactant molecules  
28 chosen allowed the investigation of the effects of chain length, head group properties and degree of unsaturation  
29 on the reaction kinetics as well as the proportion of surface-active products formed. NR experiments together  
30 with tailored kinetic modelling allowed us to determine the rate coefficients for the oxidation of OA, POA and  
31 MO monolayers to be  $(2.8 \pm 0.7) \times 10^{-8} \text{ cm}^2 \text{ molecule}^{-1} \text{ s}^{-1}$ ,  $(2.4 \pm 0.5) \times 10^{-8} \text{ cm}^2 \text{ molecule}^{-1} \text{ s}^{-1}$  and  $(3.3 \pm$   
32  $0.6) \times 10^{-8} \text{ cm}^2 \text{ molecule}^{-1} \text{ s}^{-1}$ , respectively. The corresponding uptake coefficients were found to be  $(2.1 \pm 0.5)$   
33  $\times 10^{-3}$ ,  $(1.7 \pm 0.3) \times 10^{-3}$  and  $(2.1 \pm 0.4) \times 10^{-3}$ . For the much slower  $\text{NO}_3$ -initiated oxidation of the saturated  
34 surfactant SA we obtained a rate coefficient of  $(5 \pm 1) \times 10^{-12} \text{ cm}^2 \text{ molecule}^{-1} \text{ s}^{-1}$  leading to an uptake  
35 coefficient of  $(5 \pm 1) \times 10^{-7}$ .

36

37 Our investigations demonstrate that  $\text{NO}_3$  will make a substantial contribution to the processing of unsaturated  
38 surfactants at the air–water interface during the night given its reactivity is ca. two orders of magnitude higher  
39 than that of  $\text{O}_3$ . Furthermore, the relative contributions of  $\text{NO}_3$  and  $\text{O}_3$  to the oxidative losses vary massively  
40 between structurally closely related species:  $\text{NO}_3$  reacts  $\sim 384$  times faster than  $\text{O}_3$  with the most common model





1 surfactant OA, but only ~ 58 times faster with its methyl ester MO. It is therefore required to perform a case-by-  
2 case assessment of the relative contributions of the different degradation routes for any specific surfactant. The  
3 impact of NO<sub>3</sub> on the fate of saturated surfactants is slightly less well quantified given the limited kinetic data,  
4 but NO<sub>3</sub> is very likely to be a key contributor to the loss of saturated species at night-time taking over from OH-  
5 dominated loss during the day.

6  
7 The retention of the organic character at the air–water interface also differs fundamentally between the surfactant  
8 species studied. On the one hand, the fatty acids (OA and POA) form products stable at the air–water interface  
9 with yields of ~ 15–20%. On the other hand, NO<sub>3</sub>-initiated oxidation of the oleic acid methyl ester MO rapidly  
10 removes the organic character from the surface of the aqueous droplet (≤ 3% surface-active products). The film-  
11 forming potential of reaction products will thus depend on the relative proportions of saturated and unsaturated  
12 surfactants as well as the head group properties.

13  
14 The lifetime with respect to NO<sub>3</sub>-initiated oxidation of an organic monolayer of monounsaturated molecules is  
15 about 5 to 7 minutes, while it becomes about 2<sup>1</sup> days for saturated species. Actual atmospheric residence times of  
16 unsaturated species are much longer than the lifetimes determined with respect to their reactions at the air–water  
17 interface, so it follows that they must be protected from oxidative attack *e.g.* by incorporation into a complex  
18 aerosol matrix or in mixed surface films with yet unexplored kinetic behaviour.

19

## 20 Acknowledgements

21 The authors are grateful to Prof. Ulrich Pöschl and Dr Manabu Shiraiwa for expert advice on the PRA  
22 modelling. The authors would like to thank Dr Francesco Piscitelli and Dr Ernesto Scoppola for the help during  
23 the night shifts on FIGARO. We would like to thank the Partnership for Soft Condensed Matter for access to the  
24 ellipsometer, and the ILL (Grenoble, France) for allocations of beam time on FIGARO. FS is grateful for  
25 support from the ILL and the University of Reading in the framework of the NEATNOx studentship. KR is  
26 grateful to NERC for his studentship. CP thanks NERC (grant number NE/G000883/1) for support.

27

## 28 References

- 29 Adams, E. & Allen, H. Palmitic Acid on Salt Subphases and in Mixed Monolayers of Cerebrosides: Application  
30 to Atmospheric Aerosol Chemistry. *Atmosphere (Basel)*, **4**, 315–336 (2013).
- 31 Allan, J. D. *et al.* Contributions from transport, solid fuel burning and cooking to primary organic aerosols in  
32 two UK cities. *Atmos. Chem. Phys.* **10**, 647–668 (2010).
- 33 Allodi, G., FMINUIT - A binding to Minuit for Matlab, Octave & Scilab.
- 34 Campbell, R., Wacklin, H., Sutton, I., Cubitt, R. & Fragneto, G. FIGARO: The new horizontal neutron  
35 reflectometer at the ILL. *Eur. Phys. J. Plus* **126**, 107 (2011).
- 36 Campbell, R. A., Tummino, A., Noskov, B. A. & Varga, I. Polyelectrolyte/surfactant films spread from neutral  
37 aggregates. *Soft Matter* **12**, 5304–5312 (2016).
- 38 Ciumac, D. *et al.* Implications of lipid monolayer charge characteristics on their selective interactions with a  
39 short antimicrobial peptide. *Colloids Surfaces B Biointerfaces* **150**, 308–316 (2017).
- 40 Compernelle, S., Ceulemans, K. & Müller, J.-F. EVAPORATION: a new vapour pressure estimation method for  
41 organic molecules including non-additivity and intramolecular interactions. *Atmos. Chem. Phys.* **11**,  
42 9431–9450 (2011).

43



- 1
- 2 Cosman, L. M., Knopf, D. A. & Bertram, A. K. N<sub>2</sub>O<sub>5</sub> Reactive Uptake on Aqueous Sulfuric Acid Solutions  
3 Coated with Branched and Straight-Chain Insoluble Organic Surfactants. *J. Phys. Chem. A* **112**, 2386–  
4 2396 (2008a).
- 5 Cosman, L. M. & Bertram, A. K. Reactive Uptake of N<sub>2</sub>O<sub>5</sub> on Aqueous H<sub>2</sub>SO<sub>4</sub> Solutions Coated with 1-  
6 Component and 2-Component Monolayers. *J. Phys. Chem. A* **112**, 4625–4635 (2008b).
- 7 Docherty, K. S. & Ziemann, P. J. Reaction of Oleic Acid Particles with NO<sub>3</sub> Radicals: Products, Mechanism,  
8 and Implications for Radical-Initiated Organic Aerosol Oxidation. *J. Phys. Chem. A* **110**, 3567–3577  
9 (2006).
- 10 Estillore, A. D., Trueblood, J. V & Grassian, V. H. Atmospheric chemistry of bioaerosols: heterogeneous and  
11 multiphase reactions with atmospheric oxidants and other trace gases. *Chem. Sci.* **7**, 6604–6616 (2016).
- 12 Fu, P. Q., Kawamura, K., Chen, J., Charrière, B. & Sempéré, R. Organic molecular composition of marine  
13 aerosols over the Arctic Ocean in summer: contributions of primary emission and secondary aerosol  
14 formation. *Biogeosciences* **10**, 653–667 (2013).
- 15 Fuzzi, S. *et al.* Critical assessment of the current state of scientific knowledge, terminology, and research needs  
16 concerning the role of organic aerosols in the atmosphere, climate, and global change. *Atmos. Chem.*  
17 *Phys.* **6**, 2017–2038 (2006).
- 18 Gilman, J. B., Eliason, T. L., Fast, A. & Vaida, V. Selectivity and stability of organic films at the air–aqueous  
19 interface. *J. Colloid Interface Sci.* **280**, 234–243 (2004).
- 20 Gross, S., Iannone, R., Xiao, S. & Bertram, A. K. Reactive uptake studies of NO<sub>3</sub> and N<sub>2</sub>O<sub>5</sub> on alkenoic acid,  
21 alkanolate, and polyalcohol substrates to probe nighttime aerosol chemistry. *Phys. Chem. Chem. Phys.*  
22 **11**, 7792–7803 (2009).
- 23 Gross, S. & Bertram, A. K. Products and kinetics of the reactions of an alkane monolayer and a terminal alkene  
24 monolayer with NO<sub>3</sub> radicals. *J. Geophys. Res. Atmos.* **114**, (2009).
- 25 Hearn, J. D., Lovett, A. J. & Smith, G. D. Ozonolysis of oleic acid particles: evidence for a surface reaction and  
26 secondary reactions involving Criegee intermediates. *Phys. Chem. Chem. Phys.* **7**, 501–511 (2005).
- 27 Huff Hartz, K. E., Weitkamp, E. A., Sage, A. M., Donahue, N. M. & Robinson, A. L. Laboratory measurements  
28 of the oxidation kinetics of organic aerosol mixtures using a relative rate constants approach. *J. Geophys.*  
29 *Res.* **112**, D04204 (2007).
- 30 Hung, H. M., Katrib, Y. & Martin, S. T. Products and mechanisms of the reaction of oleic acid with ozone and  
31 nitrate radical. *J. Phys. Chem. A* **109**, 4517–4530 (2005).
- 32 Jones, S. H. *et al.* Are organic films from atmospheric aerosol and sea water inert to oxidation by ozone at the  
33 air–water interface? *Atmos. Environ.* **161**, 274–287 (2017).
- 34 King, M. D., Thompson, K. C. & Ward, A. D. Laser Tweezers Raman Study of Optically Trapped Aerosol  
35 Droplets of Seawater and Oleic Acid Reacting with Ozone: Implications for Cloud-Droplet Properties. *J.*  
36 *Am. Chem. Soc.* **126**, 16710–16711 (2004).
- 37 King, M. D. *et al.* Oxidation of oleic acid at the air–water interface and its potential effects on cloud critical  
38 supersaturations. *Phys. Chem. Chem. Phys.* **11**, 7699–7707 (2009).
- 39 King, M. D., Rennie, A. R., Pfrang, C., Hughes, A. V & Thompson, K. C. Interaction of nitrogen dioxide (NO<sub>2</sub>)  
40 with a monolayer of oleic acid at the air–water interface – A simple proxy for atmospheric aerosol.  
41 *Atmos. Environ.* **44**, 1822–1825 (2010).
- 42 Knopf, D. A., Anthony, L. M. & Bertram, A. K. Reactive Uptake of O<sub>3</sub> by Multicomponent and Multiphase  
43 Mixtures Containing Oleic Acid. *J. Phys. Chem. A* **109**, 5579–5589 (2005).
- 44 Knopf, D. A., Mak, J., Gross, S. & Bertram, A. K. Does atmospheric processing of saturated hydrocarbon  
45 surfaces by NO<sub>3</sub> lead to volatilization? *Geophys. Res. Lett.* **33**, (2006).
- 46 Knopf, D. A., Cosman, L. M., Mousavi, P., Mokamati, S. & Bertram, A. K. A Novel Flow Reactor for Studying  
47 Reactions on Liquid Surfaces Coated by Organic Monolayers: Methods, Validation, and Initial Results.  
48 *J. Phys. Chem. A* **111**, 11021–11032 (2007).
- 49 Knopf, D. A., Forrester, S. M. & Slade, J. H. Heterogeneous oxidation kinetics of organic biomass burning  
50 aerosol surrogates by O<sub>3</sub>, NO<sub>2</sub>, N<sub>2</sub>O<sub>5</sub>, and NO<sub>3</sub>. *Phys. Chem. Chem. Phys.* **13**, 21050–21062 (2011).
- 51



- 1 Kuhne, R., Ebert, R.-U., Kleint, F., Schmidt, G. & Schuurmann, G. Group Contribution Methods to Estimate  
2 Water Solubility of Organic Chemicals. *Chemosphere* **30**, 2061–2077 (1995).
- 3 Lu, J. R., Thomas, R. K. & Penfold, J. Surfactant layers at the air/water interface: structure and composition.  
4 *Adv. Colloid Interface Sci.* **84**, 143–304 (2000).
- 5 MATLAB. *version 7.12.0 (R2011a)*. (The Math Works Inc., 2011).
- 6 Moise, T. & Rudich, Y. Uptake of Cl and Br by organic surfaces-A perspective on organic aerosols processing  
7 by tropospheric oxidants. *Geophys. Res. Lett.* **28**, 4083–4086 (2001).
- 8 Moise, T., Talukdar, R. K., Frost, G. J., Fox, R. W. & Rudich, Y. Reactive uptake of NO<sub>3</sub> by liquid and frozen  
9 organics. *J. Geophys. Res. Atmos.* **107**, AAC 6-1–AAC 6-9 (2002).
- 10 Mora-Diez, N. & Boyd, R. J. A Computational Study of the Kinetics of the NO<sub>3</sub> Hydrogen-Abstraction Reaction  
11 from a Series of Aldehydes (XCHO: X = F, Cl, H, CH<sub>3</sub>). *J. Phys. Chem. A* **106**, 384–394 (2002).
- 12 Morris, J. W. *et al.* Kinetics of submicron oleic acid aerosols with ozone: A novel aerosol mass spectrometric  
13 technique. *Geophys. Res. Lett.* **29**, 71–74 (2002).
- 14 Ng, N. L. *et al.* Nitrate radicals and biogenic volatile organic compounds: oxidation, mechanisms, and organic  
15 aerosol. *Atmos. Chem. Phys.* **17**, 2103–2162 (2017).
- 16 Ots, R. *et al.* Model simulations of cooking organic aerosol (COA) over the UK using estimates of emissions  
17 based on measurements at two sites in London. *Atmos. Chem. Phys.* **16**, 13773–13789 (2016).
- 18 Pfrang, C., Shiraiwa, M. & Pöschl, U. Coupling aerosol surface and bulk chemistry with a kinetic double layer  
19 model (K2-SUB): oxidation of oleic acid by ozone. *Atmos. Chem. Phys.* **10**, 4537–4557 (2010).
- 20 Pfrang, C., Shiraiwa, M. & Pöschl, U. Chemical ageing and transformation of diffusivity in semi-solid multi-  
21 component organic aerosol particles. *Atmos. Chem. Phys.* **11**, 7343–7354 (2011).
- 22 Pfrang, C. *et al.* Ozonolysis of methyl oleate monolayers at the air–water interface: oxidation kinetics, reaction  
23 products and atmospheric implications. *Phys. Chem. Chem. Phys.* **16**, 13220–13228 (2014).
- 24 Pöschl, U., Rudich, Y. & Ammann, M. Kinetic model framework for aerosol and cloud surface chemistry and  
25 gas-particle interactions - Part 1: General equations, parameters, and terminology. *Atmos. Chem. Phys.* **7**,  
26 5989–6023 (2007).
- 27 Robinson, A. L., Donahue, N. M. & Rogge, W. F. Photochemical oxidation and changes in molecular  
28 composition of organic aerosol in the regional context. *J. Geophys. Res. Atmos.* **111** (2006).
- 29 Sebastiani, F., Campbell, R. A. & Pfrang, C. Complementarity of neutron reflectometry and ellipsometry for the  
30 study of atmospheric reactions at the air–water interface. *RSC Adv.* **5**, 107105–107111 (2015).
- 31 Seddon, A. M. *et al.* Control of Nanomaterial Self-Assembly in Ultrasonically Levitated Droplets. *J. Phys.*  
32 *Chem. Lett.* **7**, 1341–1345 (2016).
- 33 Seinfeld, J. H. & Pandis, S. N. *Atmospheric Chemistry and Physics: From Air Pollution to Climate Change*.  
34 (John Wiley & Sons, Inc., 2006).
- 35 Shastri, L. V & Huie, R. E. Rate constants for Hydrogen abstraction reactions of NO<sub>3</sub> in aqueous solution. *Int. J.*  
36 *Chem. Kinet.* **22**, 505–512 (1990).
- 37 Shindell, D. T. *et al.* Improved Attribution of Climate Forcing to Emissions. *Science* **326** (5953), 716–718  
38 (2009).
- 39 Shiraiwa, M., Garland, R. M. & Pöschl, U. Kinetic double-layer model of aerosol surface chemistry and gas-  
40 particle interactions (K2-SURF): Degradation of polycyclic aromatic hydrocarbons exposed to O<sub>3</sub>, NO<sub>2</sub>,  
41 H<sub>2</sub>O, OH and NO<sub>3</sub>. *Atmos. Chem. Phys.* **9**, 9571–9586 (2009).
- 42 Shiraiwa, M., Pfrang, C. & Pöschl, U. Kinetic multi-layer model of aerosol surface and bulk chemistry (KM-  
43 SUB): the influence of interfacial transport and bulk diffusion on the oxidation of oleic acid by ozone.  
44 *Atmos. Chem. Phys.* **10**, 3673–3691 (2010).
- 45 Shiraiwa, M., Ammann, M., Koop, T. & Pöschl, U. Gas uptake and chemical aging of semisolid organic aerosol  
46 particles. *Proc. Natl. Acad. Sci.* **108**, 11003–11008 (2011).
- 47 Shiraiwa, M., Pfrang, C., Koop, T. & Pöschl, U. Kinetic multi-layer model of gas-particle interactions in  
48 aerosols and clouds (KM-GAP): linking condensation, evaporation and chemical reactions of organics,  
49 oxidants and water. *Atmos. Chem. Phys.* **12**, 2777–2794 (2012a).
- 50



- 1 Shiraiwa, M., Pöschl, U. & Knopf, D. A. Multiphase Chemical Kinetics of NO<sub>3</sub> Radicals Reacting with Organic  
2 Aerosol Components from Biomass Burning. *Environ. Sci. Technol.* **46**, 6630–6636 (2012b).
- 3 Shiraiwa, M., Zuend, A., Bertram, A. K. & Seinfeld, J. H. Gas-particle partitioning of atmospheric aerosols:  
4 interplay of physical state, non-ideal mixing and morphology. *Phys. Chem. Chem. Phys.* **15**, 11441–  
5 11453 (2013).
- 6 Skoda, M. W. A., Thomas, B., Hagreen, M., Sebastiani, F. & Pfrang, C. Simultaneous neutron reflectometry and  
7 infrared reflection absorption spectroscopy (IRRAS) study of mixed monolayer reactions at the air–  
8 water interface. *RSC Adv.* **7**, 34208–34214 (2017).
- 9 Smith, G. D., Woods, E., DeForest, C. L., Baer, T. & Miller, R. E. Reactive Uptake of Ozone by Oleic Acid  
10 Aerosol Particles: Application of Single-Particle Mass Spectrometry to Heterogeneous Reaction  
11 Kinetics. *J. Phys. Chem. A* **106**, 8085–8095 (2002).
- 12 Sobanska, S. *et al.* Influence of stearic acid coating of the NaCl surface on the reactivity with NO<sub>2</sub> under  
13 humidity. *Phys. Chem. Chem. Phys.* **17**, 10963–10977 (2015).
- 14 Stevens, B. & Feingold, G. Untangling aerosol effects on clouds and precipitation in a buffered system. *Nature*  
15 **461**, 607–613 (2009).
- 16 Stocker, T. F. *et al.* Contribution of Working Group I to the Fifth Assessment Report of the Intergovernmental  
17 Panel on Climate Change. in ‘*Climate Change 2013: The Physical Science Basis*’ (Cambridge  
18 University Press, 2013). doi:10.1017/CBO9781107415324
- 19 Tervahattu, H., Juhanaja, J. & Kupiainen, K. Identification of an organic coating on marine aerosol particles by  
20 TOF-SIMS. *J. Geophys. Res. Atmos.* **107**, ACH 18-1–ACH 18-7 (2002a).
- 21 Tervahattu, H. *et al.* New evidence of an organic layer on marine aerosols. *J. Geophys. Res. Atmos.* **107**, AAC 1-  
22 1–AAC 1-8 (2002b).
- 23 Thompson, K. C. *et al.*, Reaction of a phospholipid monolayer with gas-phase ozone at the air-water interface:  
24 measurement of surface excess and surface pressure in real time. *Langmuir*, **26**, 17295–303 (2010).
- 25 Thompson, K. C. *et al.* Degradation and Rearrangement of a Lung Surfactant Lipid at the Air–Water Interface  
26 during Exposure to the Pollutant Gas Ozone. *Langmuir* **29**, 4594–4602 (2013).
- 27 Vesna, O. *et al.* Changes of fatty acid aerosol hygroscopicity induced by ozonolysis under humid conditions.  
28 *Atmos. Chem. Phys.* **8**, 4683–4690 (2008).
- 29 Virtanen, A. *et al.* An amorphous solid state of biogenic secondary organic aerosol particles. *Nature* **467**, 824–  
30 827 (2010).
- 31 Wadia, Y., Tobias, D. J., Stafford, R. & Finlayson-Pitts, B. J. Real-Time Monitoring of the Kinetics and Gas-  
32 Phase Products of the Reaction of Ozone with an Unsaturated Phospholipid at the Air–Water Interface.  
33 *Langmuir* **16**, 9321–9330 (2000).
- 34 Wang, Y., Cannon, F. S., Salama, M., Fonseca, D. A. & Giese, S. Characterization of Pyrolysis Products from a  
35 Biodiesel Phenolic Urethane Binder. *Environ. Sci. Technol.* **43**, 1559–1564 (2009).
- 36 Wayne, R. P. *et al.* The nitrate radical: Physics, chemistry, and the atmosphere. *Atmos. Environ. Part A. Gen.*  
37 *Top.* **25**, 1–203 (1991).
- 38 Xiao, S. & Bertram, A. K. Reactive uptake kinetics of NO<sub>3</sub> on multicomponent and multiphase organic mixtures  
39 containing unsaturated and saturated organics. *Phys. Chem. Chem. Phys.* **13**, 6628–6636 (2011).
- 40 Zahardis, J. & Petrucci, G. A. The oleic acid-ozone heterogeneous reaction system: products, kinetics, secondary  
41 chemistry, and atmospheric implications of a model system – a review. *Atmos. Chem. Phys.* **7**, 1237–  
42 1274 (2007).
- 43 Zhang, Y. *et al.* Gas-surface reactions of nitrate radicals with vinyl-terminated self-assembled monolayers. *Phys.*  
44 *Chem. Chem. Phys.* **16**, 16659–16670 (2014).
- 45 Zhao, Z., Husainy, S., Stoudemayer, C. T. & Smith, G. D. Reactive uptake of NO<sub>3</sub> radicals by unsaturated fatty  
46 acid particles. *Phys. Chem. Chem. Phys.* **13**, 17809–17817 (2011).
- 47 Ziemann, P. J. Aerosol products, mechanisms, and kinetics of heterogeneous reactions of ozone with oleic acid  
48 in pure and mixed particles. *Faraday Discuss.* **130**, 469–490 (2005).
- 49